J. Mech. Phys. Solids 214 (2026) 106663

Contents lists available at ScienceDirect

Journal of the Mechanics and Physics of Solids

journal homepage: www.elsevier.com/locate/jmps

On rubber elasticity from a microscale structural mechanics representation of polymer chains

Matteo Pelliciari *, Stefano Sirotti, Angelo Marcello Tarantino

Department of Engineering "Enzo Ferrari", University of Modena and Reggio Emilia, via P. Vivarelli 10, 41125, Modena, Italy

ARTICLE INFO

Keywords:
Hyperelasticity
Nonlinear mechanics
Micro-to-macro modeling
Network-averaging
Strain-energy function

ABSTRACT

The search for a comprehensive strain-energy function for isotropic rubber elasticity has long been a central topic in continuum mechanics. Despite extensive effort and a variety of approaches, this problem remains open and continues to stimulate theoretical developments. In this contribution, we present a further attempt to address this longstanding challenge based on a microscale structural mechanics representation of polymer chains. Chain elasticity is derived from the strain energy associated with deformation of the (micro)structure, rather than from configurational entropy as in classical statistical mechanics approaches. The resulting force–extension response reflects two characteristic features: (i) progressive reduction of entanglement constraints at low-to-moderate stretches; and (ii) finite chain extensibility as the locking stretch is approached. By performing network-averaging, we derive the strain-energy function of the polymer network under both affine and non-affine kinematics. The model is assessed by fitting multiaxial experimental data from several rubbers with distinct behaviors, demonstrating consistent predictive capability. The proposed microscale nonlinear mechanics framework is entirely analytical and maintains connections with fundamental principles of non-Gaussian statistical mechanics, establishing a foundation for future theoretical developments in rubber elasticity.

1. Introduction

Rubber-like materials are widely employed in engineering because of their ability to undergo large elastic deformations. Capturing this distinctive mechanical response remains a challenging task and continues to motivate the development of advanced constitutive theories, most commonly formulated within the framework of hyperelasticity.

Existing hyperelastic models for rubber materials are generally classified into two broad families (Dal et al., 2021). On one side, *phenomenological models* describe the material behavior through mathematical forms of the strain-energy function expressed in terms of invariants or principal stretches, calibrated to reproduce experimental stress–strain data from standard loading conditions. On the other side, *micromechanical models* seek a closer connection with the underlying physics of polymers. They account for molecular-scale mechanisms and network geometry using concepts from statistical mechanics.

Micromechanically based models are generally preferred because they rely on mechanisms emerging from the material microstructure. A classical and widely adopted approach is based on the non-Gaussian treatment of long-chain polymer molecules, from which the configurational entropy and the associated free energy are derived. A comprehensive exposition of this theory can be found in the book by Treloar (1975).

* Corresponding author.
E-mail addresses: matteo.pelliciari@unimore.it (M. Pelliciari), stefano.sirotti@unimore.it (S. Sirotti), angelomarcello.tarantino@unimore.it (A.M. Tarantino).

https://doi.org/10.1016/j.jmps.2026.106663
Received 4 February 2026; Received in revised form 17 April 2026; Accepted 29 April 2026
Available online 1 May 2026

A number of hyperelastic models grounded in non-Gaussian statistical mechanics have been proposed and continue to be the subject of active research and refinement. Early pioneering contributions include the three-chain model introduced by James and Guth (1943) and the four-chain model proposed by Flory and Rehner (1943). These were later followed by the well-known eight-chain model of Arruda and Boyce (1993), which has provided the foundation for extensive subsequent developments, including recent extensions and analytical formulations such as those presented by Khiêm and Itskov (2016) and Dal et al. (2020).

Despite the substantial effort and the long history devoted to the development of suitable strain-energy functions, a fully comprehensive description of rubber elasticity has still not been achieved. The fundamental challenge of identifying a constitutive form with a minimal yet sufficient set of parameters to capture nonlinear rubber elasticity remains unresolved. Evidence of this limitation is commonly observed in the calibration of existing models, which may accurately reproduce uniaxial tensile behavior but tend to be less accurate when simultaneously reproducing biaxial loading conditions. For extensive comparative assessments and related critical discussions, the reader is referred to the review works by Boyce and Arruda (2000), Marckmann and Verron (2006), Steinmann et al. (2012), and Dal et al. (2021).

A further complication is that a given constitutive model may provide accurate predictions for certain rubber materials while performing poorly for others (see, for instance, Ogden et al., 2004, Destrade et al., 2017, and Pelliciari et al., 2023). This variability arises from differences in the underlying polymer network, which may range from relatively homogeneous structures to networks containing many defects, entanglements, and other topological interactions, all of which influence the macroscopic response. Moreover, an additional issue concerns parameter identification based solely on standard experiments in homogeneous deformations, such as uniaxial and biaxial tensile tests. Such procedures do not guarantee reliable predictions under inhomogeneous deformation states, which are of primary relevance in engineering applications.

Motivated by the above considerations and by the ongoing search for improved strain-energy functions in rubber elasticity, this work proposes an alternative formulation to the classical statistical approach to polymer chain elasticity. In the present framework, the polymer chain is interpreted as a micromechanical structure composed of rigid bars representing Kuhn segments (Kuhn, 1934), interconnected by elastic hinges and translational springs. Within this formulation, the elasticity of the chain is not attributed to *entropic effects*, but instead arises from the *elastic energy* associated with the deformation of the structural model.

The elastic elements introduced in the (micro)structure account for the single-chain elasticity and the constraints arising from entanglements, which restrict the free stretching of the polymer chain. The geometry of the representative structural model naturally produces a *locking* response as full alignment of the rigid bars is approached, consistent with the concept of limiting chain extensibility. The resulting free energy and the associated force–extension relation, obtained from equilibrium, admit closed-form analytical expressions and do not require numerical evaluations or function approximations. By contrast, approaches based on the inverse Langevin function in the statistical mechanics of freely jointed chains adopt approximate representations (see, e.g., Cohen, 1991, Arruda and Boyce, 1993, and Horgan and Saccomandi, 2002).

From the polymer chain micromechanics model, we derive the strain-energy function of the isotropic network through *analytical network-averaging* (Beatty, 2003; Khiêm and Itskov, 2016). The predictive capability of the model is demonstrated by fitting several sets of experimental data from the literature, covering rubbers with markedly different mechanical behaviors. Simultaneous fitting is performed on biaxial test data in homogeneous deformations, as well as data from membrane inflation tests involving inhomogeneous deformations, which are particularly challenging to predict. The results show that the model provides a robust description of the observed responses and that, owing to its micromechanical foundation, the parameters exhibit a coherent connection with the polymer network structure.

The paper is organized as follows. In Section 2, we review the theoretical background and recall the basic principles of the statistical mechanics of polymer chains and polymer networks. Section 3 introduces the proposed micromechanical model and presents the derivation of the free energy of a single polymer chain. In Section 4, the strain-energy function of the isotropic network is derived by network-averaging under the assumption of *affine* deformation. Fitting results are presented in Section 5 using experimental data for different rubbers and deformation states, together with comparisons to well-established models from the literature. Section 6 extends the formulation to account for *non-affine* network deformations and illustrates a case in which the proposed extension provides accurate predictions while the affine model fails. Finally, concluding remarks are drawn in Section 7.

2. Theoretical background

In this section, we summarize the essential theoretical concepts of the elasticity of long-chain molecules and polymer networks. We also briefly review the basic equations governing isotropic hyperelastic materials.

2.1. Elasticity of polymer chains from statistical mechanics

In the statistical description of a single polymer chain, its geometric structure is idealized as a sequence of n rigid segments of length l, commonly referred to as Kuhn segments (Kuhn, 1934; Anssari-Benam and Bucchi, 2021). These segments are connected by freely rotating joints, with the polymer chain assumed to be unconstrained and to adopt random spatial orientations. The end-to-end distance in the reference configuration follows a random-walk statistics and assumes the root-mean-square value given by $r_0 = \sqrt{n}l$. The deformed chain length r may attain values up to the fully extended configuration, corresponding to the alignment of all segments and commonly referred to as the locking chain length, given by $r_L = nl$.

The entropy s of a randomly oriented freely jointed chain is defined in terms of the probability density function $p(r)$ through Boltzmann's relation $s = k_B \ln p(r)$, where k_B denotes the Boltzmann constant. For purely entropic elasticity, the free energy of the

polymer chain is given by $\psi = -Ts$, where T is the absolute temperature. Accordingly, the free energy can be written as

$$\psi = -k_B T \ln p(r). \tag{1}$$

A change in the configurational entropy associated with deformation of the polymer chain gives rise to a corresponding force f_c acting along the chain direction, defined as $f_c = \partial\psi/\partial r$.

In the Gaussian freely jointed chain model, the probability density function of the end-to-end distance follows a Gaussian distribution (Guth and Mark, 1934). This assumption leads to the following linear force–extension relation

$$f_c = \frac{3k_B T}{nl^2} r. \tag{2}$$

The Gaussian approximation is valid only when the chain extension remains small compared to its locking length ($r \ll nl$). In contrast, a non-Gaussian statistical treatment is required to account for finite chain extensibility. Accordingly, the exact distribution function over the full range $0 \le r \le nl$ was derived by Treloar (1946) and later independently by Wang and Guth (1952). For large values of n, the exact solution is approximated by the classical result of Kuhn and Grün (1942), yielding the well-known relation

$$f_c = \frac{k_B T}{l} \mathcal{L}^{-1}\left(\frac{r}{nl}\right), \tag{3}$$

where $\mathcal{L}^{-1}(x)$ denotes the inverse of the Langevin function $\mathcal{L}(x) = \coth(x) - 1/x$. The inverse Langevin function diverges as $r \to nl$, thereby capturing the finite extensibility of the polymer chain. The corresponding free energy of the non-Gaussian chain is given by

$$\psi = nk_B T \left(\frac{r}{nl} \mathcal{L}^{-1}\left(\frac{r}{nl}\right) + \ln \frac{\mathcal{L}^{-1}\left(\frac{r}{nl}\right)}{\sinh \mathcal{L}^{-1}\left(\frac{r}{nl}\right)} \right) + \psi_0, \tag{4}$$

where ψ_0 is a constant.

2.2. Continuum hyperelastic description of the polymer network

Rubber elasticity arises from the collective mechanical response of a three-dimensional network of long-chain molecules formed by occasional crosslinks between polymer chains. The network is assumed to consist of chains homogeneously distributed in all spatial directions, leading to an isotropic macroscopic material response. The elastically stored free energy per unit reference volume of the network (the *strain-energy function*) is given by the sum of the free energy contributions of all chains. Let N_c denote the number of polymer chains contained in a representative unit volume of the bulk material, then the strain-energy function is written as

$$W = \sum_{i=1}^{N_c} \psi(r_i). \tag{5}$$

Several models were developed by assuming that the network is represented by an assembly of a certain number of representative sets of chains oriented in different directions. Among these, the three-, four- and eight-chain models derived respectively by James and Guth (1943), Flory and Rehner (1943) and Arruda and Boyce (1993). Later, full network models were developed, the main approach being the microsphere method, in which a continuous distribution of chain orientations in space is considered and the network strain energy is obtained by integrating the free energy of polymer chains over the unit sphere (Treloar and Riding, 1979; Wu and Van Der Giessen, 1993; Miehe et al., 2004). This approach requires numerical integration, which may introduce errors and can be computationally unattractive when the model is intended for practical applications, such as implementation in finite element computations.

Beatty (2003) introduced an analytical approach to the micro-to-macro transition in full network models, in which the transition from polymer chains to the network response is performed by averaging the squared chain stretch over all possible orientations in space. This approach is referred to as the *full-network average-stretch* model. An extension of this concept was proposed by Khiêm and Itskov (2016), who represented each polymer chain in the network by a mean chain confined within a mean tube undergoing an average chain stretch and an average tube contraction. This framework will be referred to as *generalized network-averaging*.

Regardless of how the transition from polymer chain mechanics to the continuum network is performed, the strain-energy function of an isotropic solid may be expressed either in terms of the principal invariants of the right Cauchy–Green deformation tensor $\mathbf{C} = \mathbf{F}^T\mathbf{F}$, where $\mathbf{F}$ is the deformation gradient, or equivalently in terms of the principal stretches λ_i ($i = 1, 2, 3$):

$$W = W(I_1, I_2, I_3) = \hat{W}(\lambda_1, \lambda_2, \lambda_3), \tag{6}$$

with the principal invariants of $\mathbf{C}$ defined as

$$I_1 = \operatorname{tr}\mathbf{C}, \quad I_2 = \frac{1}{2}\left((\operatorname{tr}\mathbf{C})^2 - \operatorname{tr}(\mathbf{C}^2)\right), \quad I_3 = \det\mathbf{C} = J^2, \tag{7}$$

where $J = \det\mathbf{F}$ represents the volumetric change associated with the deformation. Note that the left Cauchy–Green deformation tensor $\mathbf{B} = \mathbf{F}\mathbf{F}^T$ shares the same principal invariants as $\mathbf{C}$. Therefore, the strain-energy function may equivalently be expressed in terms of $\mathbf{B}$.

Considering a strain-energy function written in terms of the principal invariants (7), the Cauchy stress tensor can be expressed, using the Rivlin–Ericksen representation for isotropic tensor functions (Rivlin and Ericksen, 1997), as

$$\mathbf{T} = \beta_0\mathbf{I} + \beta_1\mathbf{B} + \beta_{-1}\mathbf{B}^{-1}, \tag{8}$$

where $\mathbf{I}$ is the identity tensor and β_0, β_1, and β_{-1} are scalar *response functions* of the principal invariants, given by

$$\beta_0 = \frac{2}{J}\left(I_2\frac{\partial W}{\partial I_2} + I_3\frac{\partial W}{\partial I_3}\right), \quad \beta_1 = \frac{2}{J}\frac{\partial W}{\partial I_1}, \quad \beta_{-1} = -2J\frac{\partial W}{\partial I_2}. \tag{9}$$

The first Piola–Kirchhoff stress tensor is obtained via the transformation $\mathbf{P} = J\mathbf{T}\mathbf{F}^{-T}$. Under the assumption of incompressibility ($J = 1$), which is commonly adopted since volumetric changes in most rubbers are negligible, the above stress tensors reduce to

$$\mathbf{T} = -p\mathbf{I} + \beta_1\mathbf{B} + \beta_{-1}\mathbf{B}^{-1}, \quad \mathbf{P} = \mathbf{T}\mathbf{F}^{-T}, \tag{10}$$

where p is an indeterminate hydrostatic pressure that enforces the constraint of incompressibility.

In the general case of compressible hyperelastic materials, the strain-energy function may be expressed in the following form (Horgan and Saccomandi, 2004):

$$W = W^*\left(I_1, I_2, J\right) + U(J), \tag{11}$$

where $U(J)$ is a volumetric energy term introduced to capture the pressure–volume response of the material. Within this framework, the strain-energy function of the incompressible material, denoted by W_{inc}, is the restriction of W^* to the isochoric subspace $(I_1, I_2, 1)$, so that $W_{\text{inc}}(I_1, I_2) = W^*(I_1, I_2, 1)$.

In (11), both terms contribute to the response associated with volume changes, whether or not J appears explicitly in W^* (Bischoff et al., 2001). It is therefore convenient to decompose the strain-energy function into isochoric and volumetric contributions (Sansour, 2008), following the isochoric–volumetric split

$$W = \bar{W}(\bar{I}_1, \bar{I}_2) + U(J), \tag{12}$$

where the invariants $\bar{I}_1 = J^{-2/3}I_1$ and $\bar{I}_2 = J^{-4/3}I_2$ describe the isochoric deformation, and $U(J)$ accounts for volumetric changes. Under the incompressibility constraint, the incompressible strain-energy function reduces to $W_{\text{inc}}(I_1, I_2) = \bar{W}(\bar{I}_1, \bar{I}_2)$.

3. Microscale structural mechanics model of the polymer chain

In the following, we present an alternative formulation to the classical statistical approach to polymer chain elasticity based on configurational entropy. The present formulation interprets the long-chain molecule as a micromechanical structure, whose response is obtained by evaluating the elastic strain energy associated with elastic deformation.

As shown in the schematic representation in Fig. 1(a), the polymer network is composed of randomly oriented long-chain molecules that are cross-linked.

The chains interact through topological effects, such as entanglements, which form during polymerization. The zoomed-in view of a single polymer chain on the right-hand side of Fig. 1(a) schematically illustrates its conformation as well as the surrounding chains that are either entangled with it or pass in close proximity.

The structural model of the polymer chain is shown in Fig. 1(b), which depicts the structure in its initial (reference) configuration. The chain is modeled as a discrete structure composed of rigid bars representing Kuhn segments, interconnected by elastic hinges equipped with rotational springs and by translational springs that connect hinges along the chain axis x. The rotational and translational springs introduce, respectively, the single-chain elasticity and the constraints due to entanglements with neighboring chains, which restrict free motion. Accordingly, the springs provide elastic resistance to chain stretching, as illustrated in the current (deformed) configuration of Fig. 1(c).

The structure is composed of a periodic unit cell consisting of two bars, which repeats along the x-direction (Fig. 1(b)). This periodic arrangement forms the complete structural representation of the long-chain molecule, comprising n bars of length l. The structure does not possess torsional stiffness, as the unit cells are free to rotate about the x-axis. This condition is represented schematically by ideal ring constraints at the hinges along the x-axis, which allow unrestricted torsional motion.

In the initial configuration, the bars form an angle θ_0 with the y-axis, and an initial force f_c^0 acts along the x-axis. In the current configuration, the chain is subjected to a force f_c, and the deformed bar angle is θ. Defining $l_x^0 = l\sin\theta_0$ and $l_x = l\sin\theta$, we introduce the chain stretch along the chain axis x as

$$\lambda_c = \frac{nl_x}{nl_x^0} = \frac{\sin\theta}{\sin\theta_0}. \tag{13}$$

As discussed in Section 2.1, for freely jointed statistical chains the initial root-mean-square end-to-end distance is $r_0 = \sqrt{n}l$. By imposing the equivalence between this statistical length and the initial length of the structural chain model, one obtains

$$nl_x^0 = \sqrt{n}l, \tag{14}$$

from which the initial bar angle can be expressed as a function of the number of Kuhn segments between two crosslinks:

$$\theta_0 = \arcsin\left(\frac{1}{\sqrt{n}}\right). \tag{15}$$

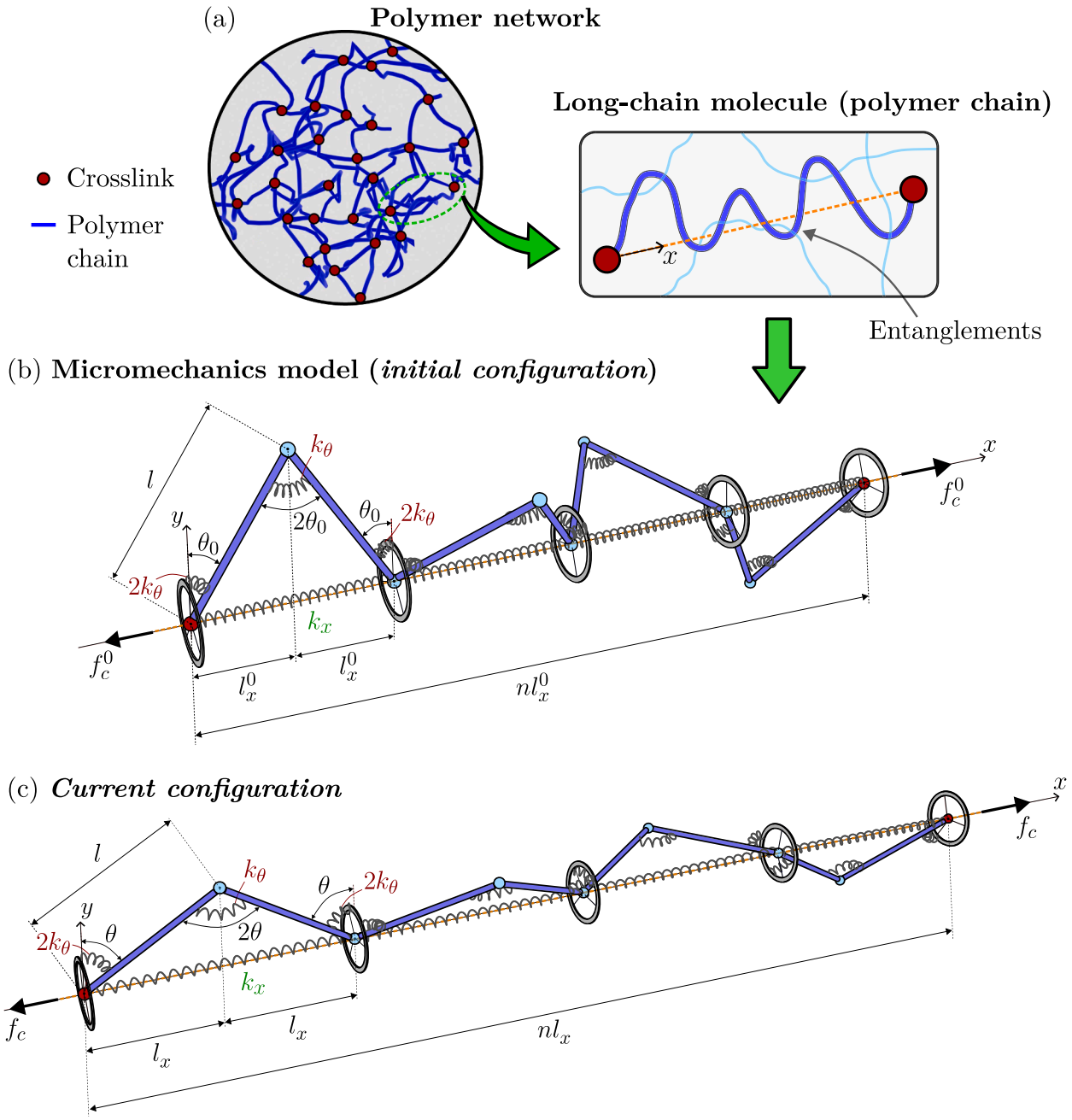

Fig. 1. (a) Schematic illustration of a polymer network and a magnified view of a single long-chain molecule between two crosslinks. (b) The chain in its initial configuration, represented as a microscale structural mechanics model. The structure consists of n rigid bars, corresponding to Kuhn segments, interconnected by elastic hinges (rotational springs) and translational springs. (c) The structure in its current configuration under an applied force f_c.

It follows from (13) that the deformed angle is linked to the chain stretch as

$$\theta = \arcsin\left(\frac{\lambda_c}{\sqrt{n}}\right). \tag{16}$$

The rotational spring connecting two bars is modeled by a harmonic potential, which captures the energetic contribution of bond-angle deformation while remaining analytically convenient (Gartner III and Jayaraman, 2019). On the other hand, the translational spring is modeled using a Morse potential (Puthur and Sebastian, 2002; Lavoie et al., 2019), which describes the nonlinear interactions and their decay at large stretches, reflecting the reduced contribution of entanglement constraints. The contributions to elastic strain

energy of rotational and translational springs are

$$\psi_\theta = \frac{n}{2}\left(\frac{k_\theta}{2}(2\theta)^2\right) + nk_\theta\theta^2 = 2nk_\theta\theta^2, \tag{17}$$

$$\psi_x = \frac{n}{2}\left(\frac{k_x}{2}\left(1-e^{-\alpha\lambda_c}\right)^2\right), \tag{18}$$

where k_x and k_θ are stiffness parameters with dimensions of energy and α is dimensionless.

The elastic strain energy stored in the structure is obtained as the sum of the contributions of the rotational and translational springs:

$$\psi_c = \psi_\theta + \psi_x = 2nk_\theta\theta^2 + \frac{n}{4}k_x\left(1-e^{-\alpha\lambda_c}\right)^2. \tag{19}$$

The total potential energy of the chain is thus defined as $\Pi_c = \psi_c - nf_c l_x$, where the second term is the work done by the external force. Equilibrium follows from the principle of stationary total potential energy and is expressed as

$$\frac{\mathrm{d}\Pi_c}{\mathrm{d}\theta} = 4nk_\theta\theta + \frac{\alpha nl}{2l_x^0}k_x e^{-\alpha\lambda_c}\left(1-e^{-\alpha\lambda_c}\right)\cos\theta - nlf_c\cos\theta = 0. \tag{20}$$

The corresponding solution yields the following expression for the force acting on the polymer chain:

$$f_c = \frac{\alpha k_x}{2l_x^0}e^{-\alpha\lambda_c}\left(1-e^{-\alpha\lambda_c}\right) + \frac{4k_\theta\theta}{l\cos\theta}. \tag{21}$$

We assume that rotational springs, accounting for single-chain elasticity, and translational springs, representing the effects of entanglements, provide comparable contributions to the elastic response in the reference configuration. We impose this by requiring that

$$\left.\frac{\partial\psi_\theta}{\partial\lambda_c}\right|_{\lambda_c=1} = \left.\frac{\partial\psi_x}{\partial\lambda_c}\right|_{\lambda_c=1} \quad \text{or, equivalently} \quad \left.\frac{\partial\psi_\theta}{\partial\theta}\right|_{\theta=\theta_0} = \left.\frac{\partial\psi_x}{\partial\theta}\right|_{\theta=\theta_0}. \tag{22}$$

Upon imposing the above condition and recalling (13), (15) and (16), the following relationship between k_x and k_θ is obtained:

$$k_x = \frac{8k_\theta e^{2\alpha}}{\alpha(e^\alpha-1)\sqrt{n-1}}\arcsin\left(\frac{1}{\sqrt{n}}\right). \tag{23}$$

Substitution into (19) and (21) yields the final expressions for the polymer chain strain energy and force

$$\psi_c = 2nk_\theta\left(\frac{e^{2\alpha}\left(1-e^{-\alpha\lambda_c}\right)^2\arcsin\left(\frac{1}{\sqrt{n}}\right)}{\alpha(e^\alpha-1)\sqrt{n-1}} + \arcsin^2\left(\frac{\lambda_c}{\sqrt{n}}\right)\right), \tag{24}$$

$$f_c = \frac{4nk_\theta}{l}\left(\frac{e^{-2\alpha(\lambda_c-1)}\left(e^{\alpha\lambda_c}-1\right)\arcsin\left(\frac{1}{\sqrt{n}}\right)}{(e^\alpha-1)\sqrt{n(n-1)}} + \frac{\arcsin\left(\frac{\lambda_c}{\sqrt{n}}\right)}{\sqrt{n\left(n-\lambda_c^2\right)}}\right). \tag{25}$$

3.1. Finite chain extensibility and comparison with the non-Gaussian freely jointed chain

The strain energy (24) endows the chain with a finitely extensible response, with elastic deformation up to the locking stretch attained when all bars align with the x-axis. This limiting stretch is $\lambda_L = \sqrt{n}$, in direct correspondence with the locking condition of the non-Gaussian theory for a freely jointed chain. This behavior is illustrated in Fig. 2, which reports the force–stretch response obtained from (25), with the force plotted in normalized form $\tilde{f_c} = \frac{3l}{4k_\theta}f_c$.

The schematic representations of the unit cell further clarify the chain behavior, illustrating that as $\lambda_c \to \lambda_L$ the bars progressively align producing strain hardening.

The proposed micromechanics chain model depends on three constitutive parameters: k_θ, α, and n. While k_θ controls the overall stiffness of the chain, the effects of n and α are illustrated in Fig. 3(a) and (b), respectively.

Since n denotes the number of bars in the chain between two crosslinks, it determines the locking stretch and therefore the strain hardening. The parameter α, instead, governs the exponential term in (25), which gives rise to the initially higher stiffness associated with entanglements. This contribution progressively weakens as the chain is stretched, reflecting a reduced mechanical contribution of entanglement constraints. The disappearance of this exponential term can be seen by writing the force in (25) as the sum of rotational and translational components,

$$f_c = \frac{4k_\theta}{3l}\left(f_\theta^* + f_x^*\right), \tag{26}$$

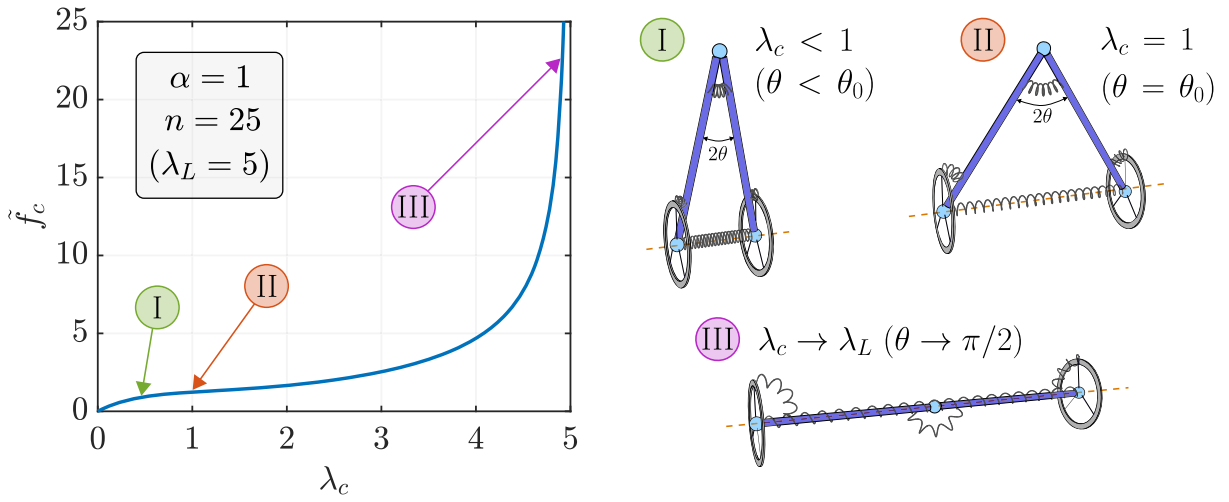

Fig. 2. Normalized force $\tilde{f}_c = \frac{3l}{4k_\theta} f_c$ versus stretch response of the micromechanics model of the polymer chain, highlighting the finite chain extensibility and the strain hardening behavior as the locking stretch $\lambda_L = \sqrt{n}$ is approached. The accompanying schematics illustrate the progressive alignment of the bars within the unit cell.

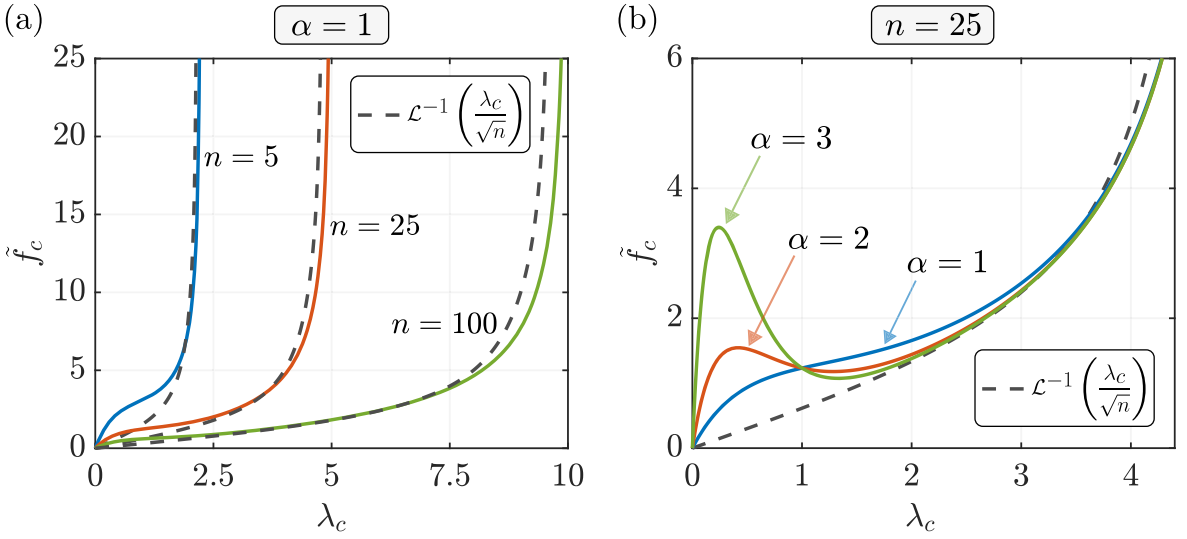

Fig. 3. Effect of (a) the number of bars n and (b) the parameter α on the force–stretch response of the chain. The parameter α controls the initial stiffness associated with entanglement constraints, whose contribution decreases with increasing stretch. The dashed curves represent the inverse Langevin function of non-Gaussian freely jointed chains. The force is normalized as $\tilde{f}_c = \frac{3l}{4k_\theta} f_c$.

with

$$f_\theta^* = \frac{3n \arcsin\left(\frac{\lambda_c}{\sqrt{n}}\right)}{\sqrt{n(n-\lambda_c^2)}}, \quad f_x^* = \frac{3n\, e^{-2\alpha(\lambda_c - 1)}\left(e^{\alpha\lambda_c} - 1\right) \arcsin\left(\frac{1}{\sqrt{n}}\right)}{(e^\alpha - 1)\sqrt{n(n-1)}}. \tag{27}$$

We can readily verify that

$$\lim_{\lambda_c \to \lambda_L} \frac{f_x^*}{f_\theta^*} = 0, \tag{28}$$

indicating that, when approaching the limiting chain extensibility, the contribution of the exponential term f_x^* becomes negligible compared to that of f_θ^*.

The form of the chain force f_c can be further understood by examining the series expansion of the rotational contribution f_θ^*, since the translational component f_x^* vanishes at large stretches. For this purpose, it is convenient to introduce the relative stretch $\eta = r/(nl) = \lambda_c/\sqrt{n}$ and write

$$f_\theta^* = \frac{3\arcsin\eta}{\sqrt{1-\eta^2}.} \tag{29}$$

Expanding in series f_θ^* in the relative stretch we have

$$f_\theta^* = 3\eta + 2\eta^3 + \frac{8}{5}\eta^5 + \frac{48}{35}\eta^7 + \cdots \tag{30}$$

The classical non-Gaussian (Langevin) freely jointed chain, whose force–extension relation is given in (3), admits the following series expansion

$$\mathcal{L}^{-1}(\eta) = 3\eta + \frac{9}{5}\eta^3 + \frac{297}{175}\eta^5 + \frac{1539}{875}\eta^7 + \cdots \tag{31}$$

The comparison between (30) and (31) reveals that the proposed chain model exhibits a functional structure analogous to the Langevin response, differing only in the coefficients that arise from the structural representation of the polymer chain.

This correspondence is evident in Fig. 3(a), where the dashed curves represent the inverse Langevin function. The qualitative agreement between its trend and that of the proposed model f_c is apparent. Note that the normalization adopted for $\tilde{f}_c = \frac{3l}{4k_\theta} f_c$ was chosen so as to match the first coefficient of the series expansion in our model and in the Langevin expression, for the purpose of a consistent comparison in the figure.

Despite the qualitative insight provided by the above discussion, accurate approximations of the response functions in finite chain extensibility models cannot be obtained through Taylor expansions. This limitation arises from the presence of a singularity as $\eta \to 1$, which precludes a global polynomial representation. Rational approximations based on Padé approximants therefore offer a suitable alternative for obtaining accurate representations and more robust physical insight (Cohen, 1991; Horgan and Saccomandi, 2002).

The aim here is not to pursue this aspect in detail, as it has already been extensively addressed in the literature. Rather, we seek to show, by means of simple rational functions, that the analytical structure of the present model is consistent with the elasticity of non-Gaussian chains. In particular, by comparing the $[1,2]$ Padé approximants of $\mathcal{L}^{-1}(\eta)$ and f_θ^*, we obtain

$$\begin{aligned} \mathcal{L}^{-1}(\eta) &\approx \frac{3\eta}{1-\frac{3}{5}\eta^2} + \mathcal{O}(\eta^4), \\ f_\theta^* &\approx \frac{3\eta}{1-\frac{2}{3}\eta^2} + \mathcal{O}(\eta^4), \end{aligned} \tag{32}$$

from which it is apparent that the two expressions share the same functional form, although the location of the singularity differs. The fact that the singularity does not occur at $\eta = 1$ is a consequence of the low order of the approximation employed. Indeed, increasing the order of the Padé approximation, for instance by considering a $[1,4]$ Padé approximant, yields

$$\begin{aligned} \mathcal{L}^{-1}(\eta) &\approx \frac{3\eta}{1-\frac{3}{5}\eta^2-\frac{36}{175}\eta^4} + \mathcal{O}(\eta^6), \\ f_\theta^* &\approx \frac{3\eta}{1-\frac{2}{3}\eta^2-\frac{4}{45}\eta^4} + \mathcal{O}(\eta^6), \end{aligned} \tag{33}$$

indicating that the singularity approaches $\eta = 1$ with increasing approximation order.

3.2. Decreasing contribution of entanglement constraints at large stretch

The effect of entanglements on the freedom of motion of polymer chains is incorporated through the exponential contribution f_x^* in (27). This term primarily influences the mechanical response at small-to-moderate strains and progressively vanishes as the chain stretch increases. In particular, this behavior is governed by the exponential decay associated with the energy term

$$\left(1 - e^{-\alpha\lambda_c}\right)^2. \tag{34}$$

A similar conceptual framework was proposed by Yeoh and Fleming (1997), who observed that the mechanical response of rubber vulcanizates is governed by two distinct deformation mechanisms. One mechanism is the classical one, which produces strain hardening at large strains and is associated with the finite extensibility of network chains. The other mechanism influences the behavior at small strains and is attributed to network imperfections, such as entanglements.

With regard to this latter mechanism, Yeoh (1993) observed experimentally a decrease in the shear modulus at relatively small strains, followed by an increase at large stretches. To capture the stiffness reduction, Yeoh and Fleming (1997) introduced a phenomenological exponential correction term in the strain energy of the form

$$\frac{A}{B}\left(1 - e^{-B(I_1-3)}\right), \tag{35}$$

where A and B are material parameters. The exponential contribution (34) proposed in the present formulation exhibits the same qualitative behavior as (35). This similarity highlights the consistency between the micromechanically motivated chain-force model developed here and earlier phenomenological descriptions of rubber elasticity.

Other authors, such as Anssari-Benam (2024), have highlighted the stiffness reduction observed in several polymers based on recent experimental data, and proposed hyperelastic models with parameters that control this feature of the mechanical response. Although arising from a different functional form, the parameter α in the present model plays a similar role, governing the transition from the initial stiff regime to the subsequent softer nonlinear behavior in the small-to-moderate deformation range.

4. Strain-energy function of the affine molecular network

In this section, we construct the macroscopic strain-energy function of an exactly incompressible polymer network composed of polymer chains characterized by the micromechanical model derived in the previous section. If volumetric effects are to be included to model compressible rubber behavior, a volumetric energy term $U(J)$ accounting for volume changes can be added following the isochoric–volumetric split (12).

The analytical transition from the mechanics of a single polymer chain to the macroscopic response of an isotropic crosslinked network is carried out following the generalized network-averaging proposed by Khiêm and Itskov (2016) (see Section 2.2). Each polymer chain is thus represented by a mean chain confined within a mean tube, characterized by an average chain stretch $\hat{\lambda}_c$ and an average tube contraction $\hat{v}_t$. The strain energy of the polymer network is expressed by an additive split as

$$\bar{W} = N_c\big(\psi_c(\hat{\lambda}_c) + \psi_t(\hat{v}_t)\big), \tag{36}$$

where N_c denotes the number of chains per unit volume of the bulk material. The function $\psi_c(\hat{\lambda}_c)$ represents the energy associated with the mean chain stretch, while $\psi_t(\hat{v}_t)$ accounts for the energy contribution due to the mean tube contraction.

Adopting the generalized network-averaging, we relate the above kinematic micro-variables to the corresponding average macro-variables $\langle\bar{\lambda}\rangle_2$ and $\langle\bar{v}\rangle_2$, where $\langle\bullet\rangle_2$ denotes the root-mean-square of $\bullet$ over the unit sphere $\mathcal{S}$, defined as

$$\langle\bullet\rangle_2 = \sqrt{\frac{1}{4\pi}\int_{\mathcal{S}}(\bullet)^2\, d\mathcal{S}}. \tag{37}$$

Hence, $\langle\bar{\lambda}\rangle_2$ and $\langle\bar{v}\rangle_2$ denote respectively the isochoric macro-stretch and macro-area contraction averaged over a unit sphere. In the developments of this section, an affine deformation of the network is assumed, so that the micro-variables coincide with their corresponding macroscopic counterparts, namely

$$\hat{\lambda}_c = \langle\bar{\lambda}\rangle_2, \quad \hat{v}_t = \langle\bar{v}\rangle_2. \tag{38}$$

4.1. Network energy from chain stretch

Let $\boldsymbol{m}$ denote the unit vector defining the initial orientation of a material line element $d\boldsymbol{X}$, such that $d\boldsymbol{X} = dX\boldsymbol{m}$. The deformed counterpart $d\boldsymbol{x}$ is related to $d\boldsymbol{X}$ according to

$$d\boldsymbol{x} = \bar{\mathbf{F}}d\boldsymbol{X}, \tag{39}$$

where $\bar{\mathbf{F}} = J^{-1/3}\mathbf{F}$ is the macroscopic isochoric deformation gradient. Introducing $\bar{\mathbf{C}} = \bar{\mathbf{F}}^{\mathrm{T}}\bar{\mathbf{F}}$, the macro-stretch of a material line element with orientation $\boldsymbol{m}$ is given by

$$\bar{\lambda} = \frac{dx}{dX} = \sqrt{\boldsymbol{m}\cdot\bar{\mathbf{C}}\boldsymbol{m}}. \tag{40}$$

For a randomly oriented (isotropic) ensemble of polymer chains, the network average of any scalar quantity depending on reference orientation $\boldsymbol{m}$ is expressed through the root-mean-square operator defined in (37), which takes the form

$$\langle\bullet\rangle_2 = \sqrt{\frac{1}{4\pi}\int_0^{2\pi}\int_0^{\pi}(\bullet)^2\sin\omega\, d\omega\, d\phi}, \tag{41}$$

where ω and ϕ are the spherical angles defining the direction $\boldsymbol{m} = (\sin\omega\cos\phi, \sin\omega\sin\phi, \cos\omega)$. The average macro-stretch over the unit sphere is obtained as

$$\langle\bar{\lambda}\rangle_2 = \sqrt{\frac{1}{4\pi}\int_0^{2\pi}\int_0^{\pi}\bar{\lambda}^2\sin\omega\, d\omega\, d\phi} = \sqrt{\frac{\bar{I}_1}{3}}, \tag{42}$$

where $\bar{I}_1$ is the first invariant of the isochoric Cauchy–Green deformation tensor, defined in Section 2.2.

By using (42) and the micro–macro stretch relation for an affine network $\hat{\lambda}_c = \langle\bar{\lambda}\rangle_2$, and substituting these into (24), the strain energy of the ideal network associated with chain stretching is obtained as $\bar{W}_c = N_c\psi_c(\hat{\lambda}_c)$. Before writing its explicit expression, we introduce the shear modulus μ_c of the ideal network by its definition:

$$\mu_c = 2\left.\frac{\partial\bar{W}_c}{\partial\bar{I}_1}\right|_{\bar{I}_1=3} = \frac{N_c}{3}\left.\frac{\partial\psi_c}{\partial\hat{\lambda}_c}\right|_{\hat{\lambda}_c=1} = \frac{8k_\theta n N_c}{3\sqrt{n-1}}\arcsin\left(\frac{1}{\sqrt{n}}\right). \tag{43}$$

Using the above result,[1] from (24) we may write the explicit expression of the strain energy of the ideal network as

$$\tilde{W}_c = N_c \psi_c\left(\sqrt{\frac{\bar{I}_1}{3}}\right) = \frac{3}{4}\mu_c\left(\frac{e^{2\alpha}\left(1-e^{-\alpha\sqrt{\frac{\bar{I}_1}{3}}}\right)^2}{\alpha(e^{\alpha}-1)} + \frac{\sqrt{n-1}\,\arcsin^2\left(\sqrt{\frac{\bar{I}_1}{3n}}\right)}{\arcsin\left(\frac{1}{\sqrt{n}}\right)}\right) + W_c^0, \tag{45}$$

with constant term W_c^0 introduced to guarantee energy-free reference configuration.

4.2. Network energy from tube contraction

As previously described, the mean polymer chain is assumed to be confined to a mean tube of constant diameter, reflecting topological constraints imposed by surrounding chains. The elastic energy associated with this topological constraint is treated as purely entropic. Following Doi and Edwards (1986) and Miehe et al. (2004), we carry out the hypothesis that the polymer takes a random walk confined by the tube, writing the probability distribution

$$p_t(\hat{v}_t) = p_0\, e^{-\rho\left(\frac{r_0}{d_0}\right)^2 \hat{v}_t}, \tag{46}$$

where p_0 is a normalization constant, $\hat{v}_t$ is the tube area contraction, r_0 is the unstrained end-to-end distance of the chain, d_0 is the reference tube diameter, and ρ is a geometrical factor related to the shape of the tube in the undeformed state. The free energy from the tube contraction is then derived as

$$\psi_t(\hat{v}_t) = -k_B T \ln p_t(\hat{v}_t) = \rho k_B T\left(\frac{r_0}{d_0}\right)^2 \hat{v}_t + \psi_t^0, \tag{47}$$

with constant ψ_t^0 allowing zero energy in reference configuration.

The contribution of the free energy within the network-averaging framework is obtained by averaging the macroscopic contraction of an infinitesimal area (Khiêm and Itskov, 2016; Anssari-Benam et al., 2021), as outlined below. The squared area contraction, considering an area element with unit normal $\boldsymbol{m}$, is expressed by Kearsley (1989) in terms of principal stretches as

$$\bar{v}^2 = \lambda_1^2\lambda_2^2\cos^2\omega + \lambda_3^2\sin^2\omega\left(\lambda_1^2\cos^2\phi + \lambda_2^2\sin^2\phi\right). \tag{48}$$

The root-mean-square of the area contraction is then derived as

$$\langle\bar{v}\rangle_2 = \sqrt{\frac{1}{4\pi}\int_0^{2\pi}\int_0^{\pi}\bar{v}^2\sin\omega\, d\omega\, d\phi} = \sqrt{\frac{\bar{I}_2}{3}}, \tag{49}$$

being $\bar{I}_2$ the second principal invariant of $\bar{\mathbf{C}}$.

We now use the micro–macro tube contraction relation for an affine network, $\hat{v}_t = \langle\bar{v}\rangle_2$, to express the network strain energy associated with the tube constraint as $\tilde{W}_t = N_c\psi_t(\hat{v}_t)$. Substitution of (49) into (47) yields the form

$$\tilde{W}_t = N_c\psi_t\left(\sqrt{\frac{\bar{I}_2}{3}}\right) = \mu_t\left(\sqrt{\frac{\bar{I}_2}{3}} - 1\right), \tag{50}$$

where we introduced the topological shear modulus $\mu_t = N_c\rho k_B T\left(\frac{r_0}{d_0}\right)^2$.

4.3. The total network strain energy

As shown previously, the two deformation mechanisms of chain stretching and tube contraction are captured by the strain measures $\bar{I}_1$ and $\bar{I}_2$, respectively. The additive split in (36) therefore allows the total network strain-energy function to be expressed as

$$\tilde{W} = \tilde{W}_c(\bar{I}_1) + \tilde{W}_t(\bar{I}_2) = \frac{3}{4}\mu_c\left(\frac{e^{2\alpha}\left(1-e^{-\alpha\sqrt{\frac{\bar{I}_1}{3}}}\right)^2}{\alpha(e^{\alpha}-1)} + \frac{\sqrt{n-1}\,\arcsin^2\left(\sqrt{\frac{\bar{I}_1}{3n}}\right)}{\arcsin\left(\frac{1}{\sqrt{n}}\right)}\right) + \mu_t\left(\sqrt{\frac{\bar{I}_2}{3}} - 1\right) + W_c^0. \tag{51}$$

[1] The condition (22), ensuring equal contributions of the rotational and translational springs to the chain response near the initial configuration, is equivalent to requiring identical contributions to the shear modulus of the network. In fact, recalling that $\psi_c = \psi_\theta + \psi_x$ and using (22) and (43), it follows that

$$\left.\frac{\partial\psi_\theta}{\partial\hat{\lambda}_c}\right|_{\hat{\lambda}_c=1} = \left.\frac{\partial\psi_x}{\partial\hat{\lambda}_c}\right|_{\hat{\lambda}_c=1} = \frac{3\mu_c}{2N_c}. \tag{44}$$

4.3.1. Physical consistency and constitutive restrictions

A requirement for plausibility concerns the behaviour of the incremental shear modulus, for which one may refer to the discussion in Section 2(a) in the work by Destrade et al. (2017). For an incompressible isotropic material, whose strain-energy function depends only on the deviatoric strain invariants and takes the form $W(I_1, I_2) = \tilde{W}(\bar{I}_1, \bar{I}_2)$, this quantity reduces to $\mu(I_1, I_2) = 2\left(\frac{\partial W}{\partial I_1} + \frac{\partial W}{\partial I_2}\right)$ and in the reference configuration must satisfy $\mu_0 > 0$. This guarantees compatibility with linear elasticity in the small-strain limit. For our strain-energy function (51), this requirement becomes

$$\mu_0 = \mu_c + \frac{\mu_t}{3} > 0. \tag{52}$$

As emphasized in Destrade et al. (2017), the above condition is one of the few mechanical restrictions that can be imposed a priori on a hyperelastic model, together with normalization $\tilde{W}(3,3) = 0$ and the requirement that the stress vanishes in the undeformed state. Regarding the first, as previously mentioned, we introduced the constant term W_c^0 in (51) to ensure vanishing energy in reference configuration. Regarding the second, we recall that for incompressible materials the condition of zero stress in the reference configuration is always satisfied by an appropriate choice of the Lagrange multiplier p in that configuration. Hence, we may conclude that the above requirements are fulfilled.

Further restrictions are often imposed on the constitutive behaviour of hyperelastic materials in the form of inequalities, which are postulated *a priori* to endow the response function with desirable qualitative features, rather than being derived from fundamental physical principles (Mihai and Goriely, 2017). A classical requirement, formulated by Baker and Ericksen (1954), is that the greater principal stress occurs in the direction of the greater principal stretch; that is $t_i > t_j$ whenever $\lambda_i > \lambda_j$, where t_i denote the principal Cauchy stresses, with $i, j = 1, 2, 3$. These conditions are known as the *Baker–Ericksen (BE) inequalities*.[2] For incompressible isotropic materials, they can be written in the form

$$(t_i - t_j)(\lambda_i - \lambda_j) > 0 \quad \Longleftrightarrow \quad \frac{\partial W}{\partial I_1} + \lambda_k^2 \frac{\partial W}{\partial I_2} > 0, \tag{53}$$

with $i, j, k = 1, 2, 3$ and $i \neq j \neq k$. The strict inequality applies when $\lambda_i \neq \lambda_j$, while the non-strict inequality ($\geq$) is admitted if $\lambda_i = \lambda_j$.

Truesdell and Noll (1965) proposed a restriction of the BE inequalities, providing a convenient condition that is sufficient, but not necessary, for the BE inequalities to be satisfied. These conditions are known as the *empirical (E) inequalities*. In the case of incompressible materials, they take the form

$$\frac{\partial W}{\partial I_1} > 0, \qquad \frac{\partial W}{\partial I_2} \geq 0. \tag{54}$$

These conditions are frequently assumed in the construction and fitting of hyperelastic models, as they help prevent undesirable or unphysical material responses.

Despite their widespread use, several authors have pointed out that the E inequalities are overly restrictive. Thiel et al. (2019) clarified that they are often employed as a criterion to ensure semi-invertibility of the stress–strain relation, even though weaker assumptions are already sufficient for this purpose. Experimental evidence supporting this observation is provided, for instance, by Falope et al. (2024). Based on accurate biaxial tests on different types of rubber, they observed that in some cases the condition $\partial W/\partial I_2 \geq 0$ is violated (see Fig. 5(c) of the referenced work).

In view of the foregoing, we provide below sufficient conditions on the constitutive parameters that enforce the E inequalities, with the aim of offering general guidance for avoiding unphysical responses. It should be kept in mind, however, that these conditions are not necessary, as they are more restrictive than the BE inequalities. Accordingly, by imposing the restrictions (54) on the strain-energy function (51), we obtain the following sufficient conditions for the satisfaction of the E inequalities:

$$\mu_c > 0, \quad n > \frac{I_1}{3}, \quad \alpha > 0, \quad \mu_t \geq 0. \tag{55}$$

In the present work, we use the above conditions to guide the fitting of constitutive parameters to experimental data, as they are expected to be compatible with a wide range of rubber-like material responses. However, in cases where these conditions prove too restrictive to capture the observed behavior, the fitting procedure may be extended by relaxing the constraint $\mu_t \geq 0$ and allowing μ_t to take negative values. Physical consistency can then be ensured by verifying the BE inequalities (53) *a posteriori*. We note that satisfaction of either the E or the BE inequalities also guarantees compatibility with the linear elastic limit expressed by (52).

5. Results and discussion

To assess the predictive capability of the proposed constitutive model, we present in the following fitting results based on available experimental data, together with comparisons to well-established hyperelastic models. The rubber materials considered are assumed to be incompressible. The strain-energy function $W(I_1, I_2) = \tilde{W}(\bar{I}_1, \bar{I}_2)$ is given in (51). The nominal stress tensor (first Piola–Kirchhoff stress) is computed from (10).

[2] The mechanical significance of the BE inequalities was clarified, for instance, by Marzano (1983). He showed that, for a hyperelastic body subjected to uniaxial tension, the deformation is a simple extension in the direction of the applied force if and only if the BE inequalities hold. We also note that Truesdell (1952) (Eq. 41.13a) previously derived, from similar physical arguments, inequalities that are in agreement with (53).

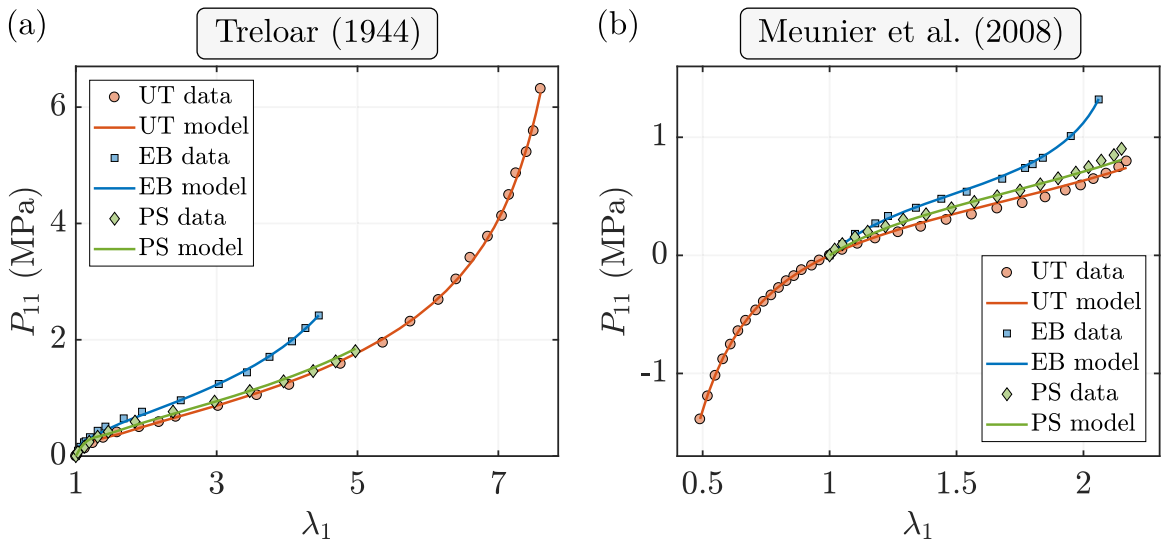

Fig. 4. Nominal stress–stretch curves obtained from simultaneous fitting of the model to the uniaxial (UT) and equibiaxial (EB) data of (a) Treloar (1944) and (b) Meunier et al. (2008). Predictions for the pure shear (PS) response using the same parameters are also shown.

5.1. Homogeneous deformations

We examine four classical homogeneous deformation modes: uniaxial tension, equibiaxial tension, biaxial tension, and pure shear. For each case, we report in Appendix A the corresponding deformation gradient and nominal stress tensor. The first set of experimental data considered is that of Treloar (1944), which provides uniaxial, equibiaxial, and pure shear tests on vulcanized rubber compounds containing 8 phr sulfur. Accurately capturing different deformation modes generally requires simultaneous fitting, as relying on uniaxial data alone is typically insufficient (Urayama, 2006). Moreover, several authors have reported that model calibration should employ experimental data spanning different regions of the attainable domain of strain invariants (Currie, 2004; Falope et al., 2024). Achieving this, however, is challenging: ideally, one would need biaxial tests performed along loading paths that adequately cover the domain, along with the inherent difficulties of conducting such experiments and accurately measuring strains and stresses.

In the following, we present a simultaneous fit in MATLAB using only data from the two boundary deformation modes of the attainable strain-invariant domain, namely uniaxial and equibiaxial tension. We then use the same set of fitted parameters to generate predictions for the additional experimental data available, which in the case of Treloar (1944) corresponds to pure shear data. Applying this procedure, we obtained the fitting parameters $\mu_c = 0.5377$ MPa, $\alpha = 27.24$, $n = 23.06$, and $\mu_t = 0.1579$ MPa. The corresponding nominal stress–stretch curves are shown in Fig. 4(a).

The model provides an excellent fit to the uniaxial and equibiaxial responses of the rubber and also yields an accurate prediction of the pure shear response, even though it was not included in the fitting.

As a further application, we performed a fitting based on the uniaxial and equibiaxial data reported by Meunier et al. (2008). The results are shown in Fig. 4(b) and correspond to parameters $\mu_c = 0.3115$ MPa, $\alpha = 0.01$, $n = 3.248$, and $\mu_t = 0.08175$ MPa. The model again provides a good description of the experimental response. A minor deviation is observed toward the end of the pure shear curve. However, given that the pure shear data were not included in the fitting process, the result remains more than satisfactory.

We applied the same fitting procedure to the data provided by Kawabata et al. (1981), obtaining parameters $\mu_c = 0.3302$ MPa, $\alpha = 0.2743$, $n = 23.724$, and $\mu_t = 0.1772$ MPa. Fig. 5(a) shows the fitting result for the uniaxial and equibiaxial data.

Using the obtained parameters, we then predicted the biaxial response for all additional biaxial tests reported by Kawabata et al. (1981), with the results shown in Fig. 5(b) and (c). The predictions are in strong agreement with the experimental data. This demonstrates that, for this dataset, fitting the model only to the two boundaries of the attainable strain invariant domain is sufficient to capture the material response for all intermediate deformation states.

A set of uniaxial tension data recently published in Pelliciari et al. (2023) was considered as an additional application, since it spans four rubber types with substantial variability in mechanical behavior. The fitting was performed using these experimental data, yielding the parameters reported in Table B.1, and the resulting curves are shown in Fig. 6.

To provide a comparison of modeling capabilities, we also considered two well-known hyperelastic models that have the same number of parameters (four) and are based on similar theoretical concepts. The first model, proposed by Khiêm and Itskov (2016), has the following strain-energy function

$$W_K = \mu_c \kappa\, n \ln \frac{\sin\left(\frac{\pi}{\sqrt{n}}\right)\left(\frac{I_1}{3}\right)^{\frac{q}{2}}}{\sin\left(\frac{\pi}{\sqrt{n}}\left(\frac{I_1}{3}\right)^{\frac{q}{2}}\right)} + \mu_t\left(\sqrt{\frac{I_2}{3}} - 1\right), \tag{56}$$

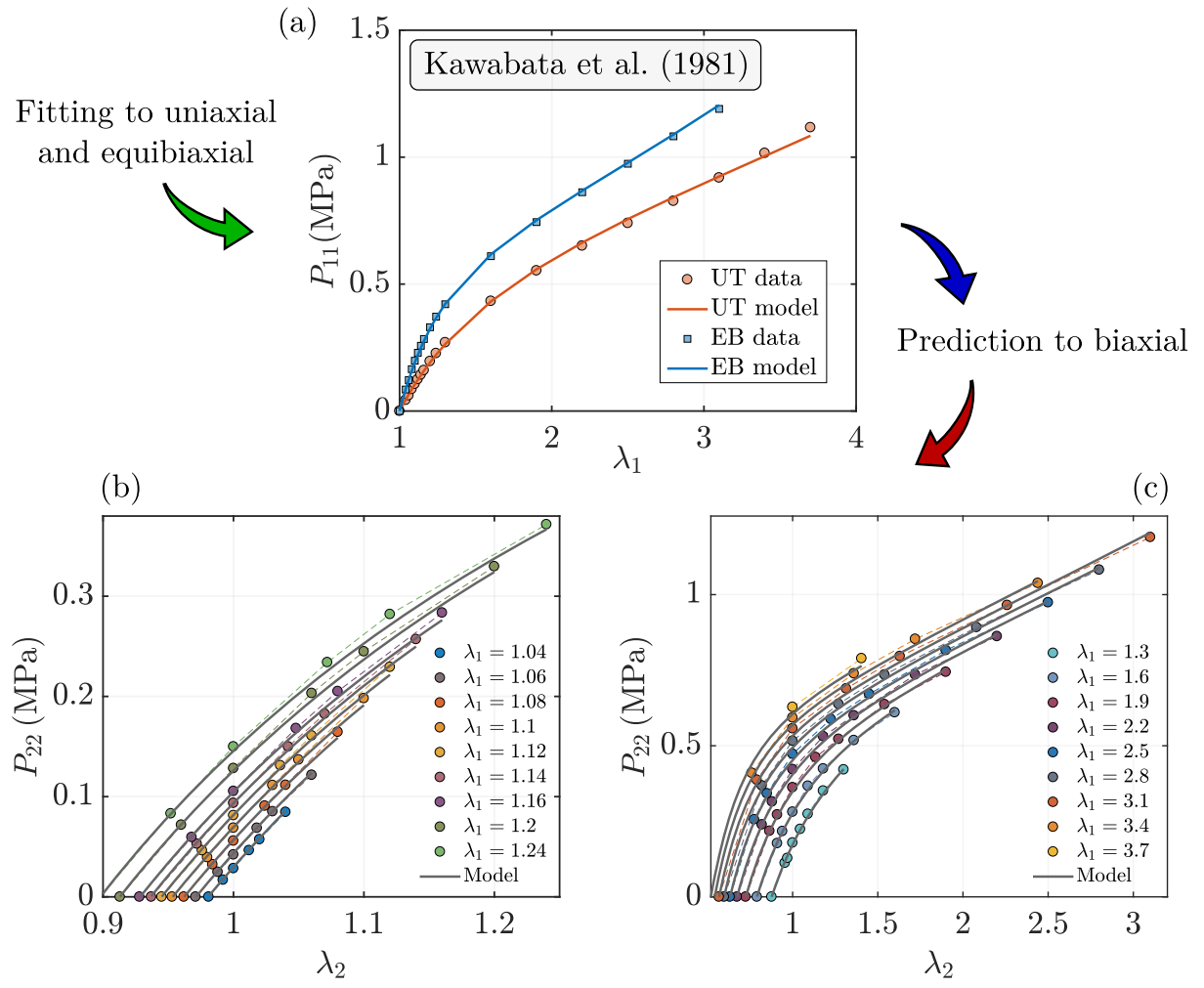

Fig. 5. (a) Nominal stress–stretch curves obtained by fitting the model to the uniaxial (UT) and equibiaxial (EB) data of Kawabata et al. (1981). Using the obtained fitting parameters, the predictions for the series of biaxial tension tests reported in Kawabata et al. (1981) are shown in figures (b) and (c).

with parameters $\mu_c\kappa$, n, q, and μ_t. The second model, proposed by Anssari-Benam (2021) and subsequently developed in Anssari-Benam and Horgan (2022), has the following form

$$W_A = \frac{3(\bar{n}-1)}{2\bar{n}}\mu N\left(\frac{I_1-3}{3N(\bar{n}-1)} - \ln\left(\frac{I_1-3N}{3-3N}\right)\right) + C_2\ln\left(\frac{I_2}{3}\right), \tag{57}$$

with parameters μ, $\bar{n}$, N, and C_2.[3] Note that for the term in I_2 we adopted a logarithmic form, as suggested in Anssari-Benam (2021) and later reported in Anssari-Benam et al. (2021), since it was found to be the most versatile among the forms analyzed by the authors.

The fitting parameters for these models were obtained and are reported in Table B.1. The resulting curves are presented in Fig. 6. In the figure, each stress–stretch curve is accompanied by the corresponding relative error with respect to the experimental measurements, defined as

$$\delta_{\text{rel}} = \frac{|P_{11}^{\text{exp}}(\lambda_{1,i}) - P_{11}(\lambda_{1,i})|}{|P_{11}^{\text{exp}}(\lambda_{1,i})|}, \tag{58}$$

where $\left(\lambda_{1,i},\ P_{11,i}^{\text{exp}}\right)$ denote the experimental stretch and nominal stress data points.

Fig. 6(a) shows that, for NR rubber, all three constitutive models reproduce the experimental response with essentially comparable accuracy across the entire deformation range. The results for silicone in Fig. 6(b) show that the present model and the Anssari-Benam

[3] Here N denotes the number of Kuhn segments. Following Anssari-Benam and Horgan (2022), the constraint $N > 1$ is relaxed and N is treated as a real-valued phenomenological parameter. In the fitting procedure, we therefore consider two separate cases, $N > 1$ and $N < 1$, and retain the solution that provides the best agreement with the data.

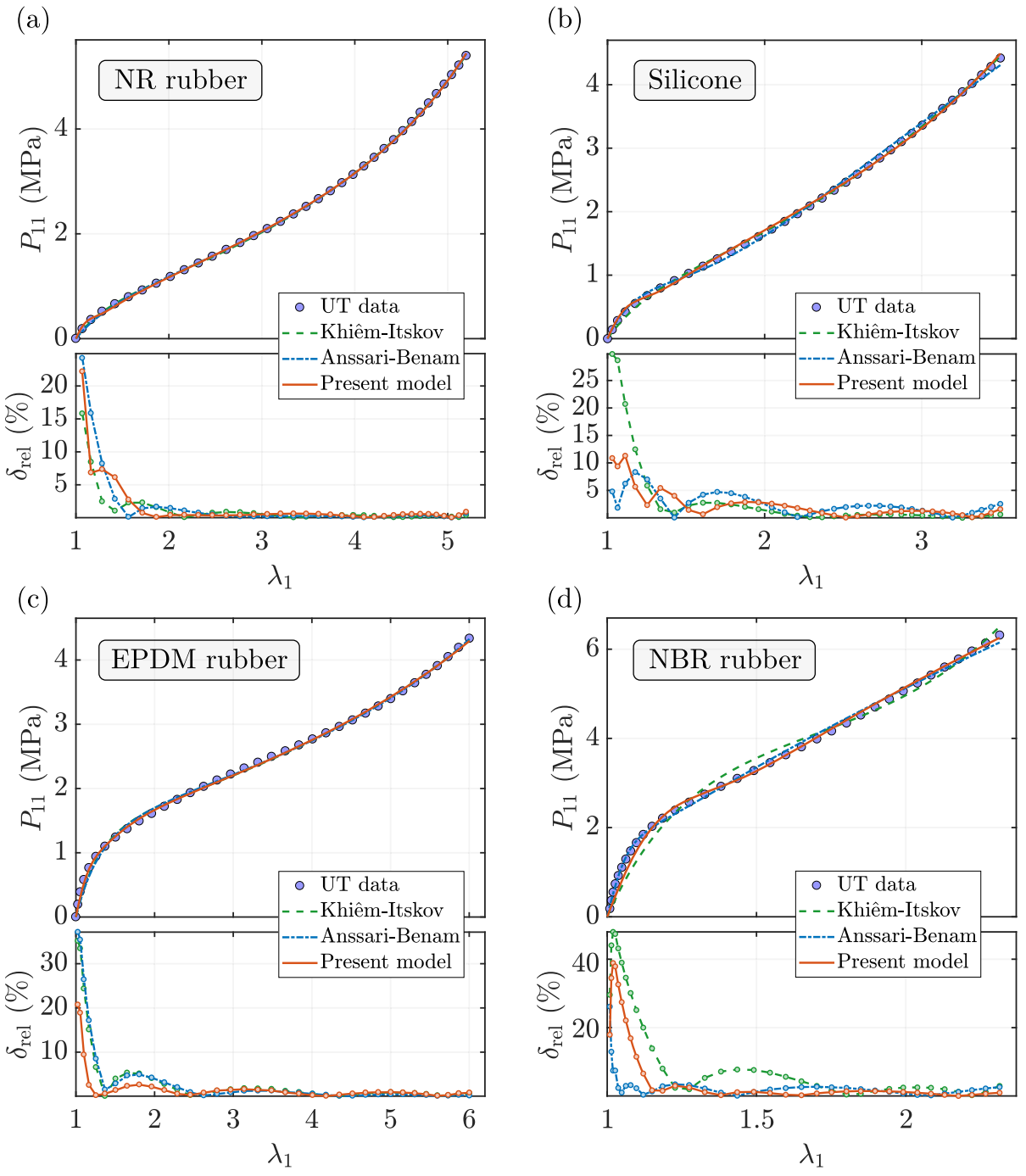

Fig. 6. Results from fitting the present model (51) and the formulations in (56) and (57), respectively proposed by Khiêm and Itskov (2016) and Anssari-Benam (2021), to the uniaxial tension data of Pelliciari et al. (2023). The corresponding plots of the relative error δ_{rel}, expressed as a percentage, are also included.

model exhibit comparable predictive capabilities, with the present model providing slightly improved accuracy at large strains. For EPDM in Fig. 6(c), the exponentially decaying term in the present model appears to be advantageous in the small-to-moderate strain regime, leading to very good agreement with the data. Finally, for NBR rubber in Fig. 6(d), the Anssari-Benam model performs significantly better at small strains, whereas the present model shows improved accuracy at large strains. In this case, both models appear to provide better agreement with the data than the Khiêm–Itskov model.

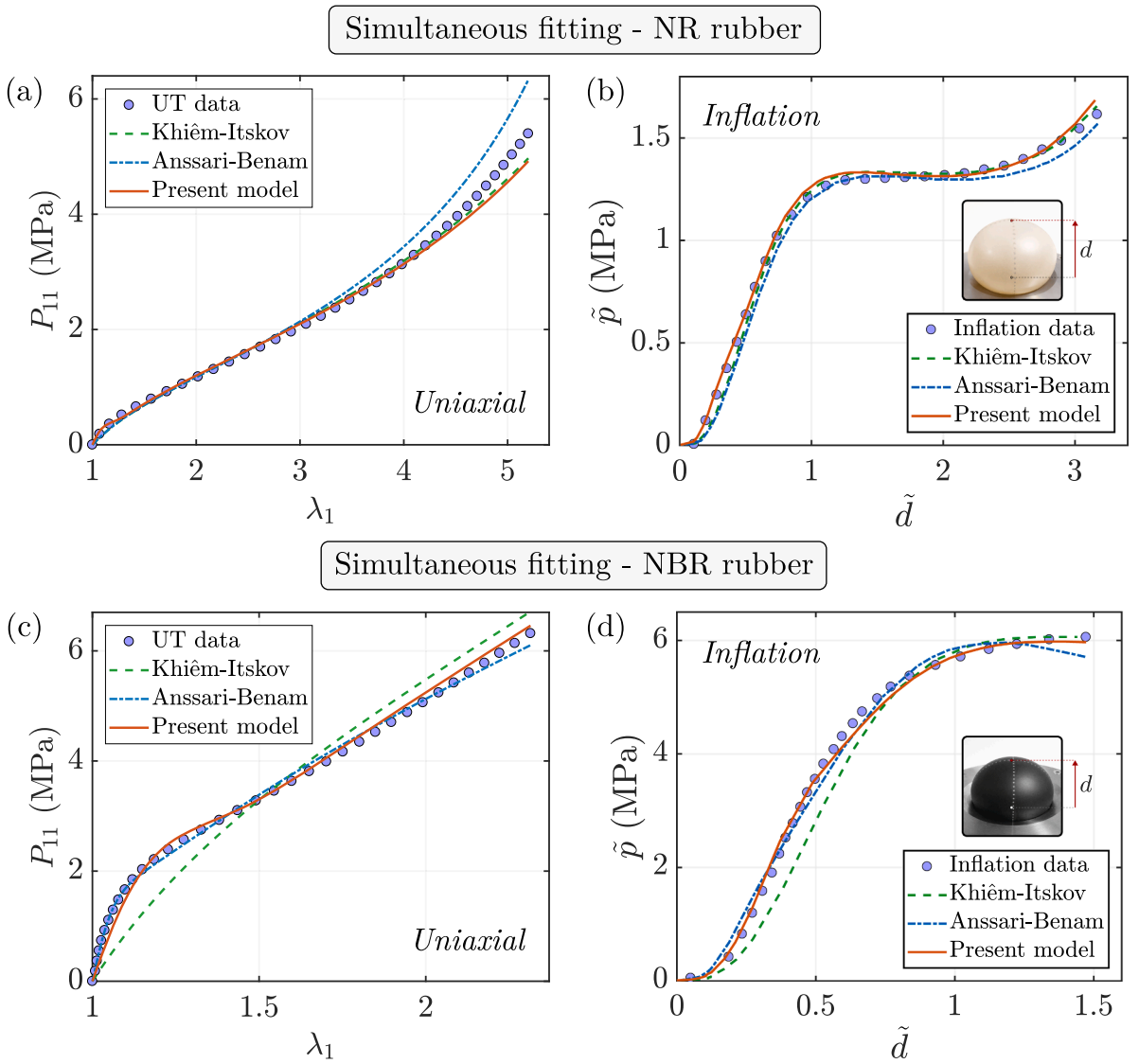

Fig. 7. Results from simultaneous fitting to uniaxial tension and biaxial membrane inflation data for (a,b) NR rubber and (c,d) NBR rubber. Uniaxial tension data are taken from Pelliciari et al. (2023). Membrane inflation data for NR rubber are taken from Sirotti et al. (2025), while those for NBR rubber were obtained in the present work under the same experimental configuration. In figures (b) and (d), deflection and pressure are normalized as $\tilde{d} = d/R$ and $\tilde{p} = p^* R/H$.

5.2. Inhomogeneous deformations

Constitutive models may perform well when calibrated on homogeneous uniaxial or biaxial test data, yet fail to provide good fitting when applied to more complex loading scenarios, such as membrane inflation or other inhomogeneous deformation tests. To examine this aspect, we apply the proposed model to a simultaneous fitting procedure involving both uniaxial and membrane inflation data.

We consider the uniaxial stress–stretch data for NR rubber reported in Pelliciari et al. (2023) together with the pressure–deflection measurements obtained from the inflation of initially flat circular membranes made of the same material, as documented in Sirotti et al. (2025). Here, the deflection d denotes the displacement measured at the center of the membrane under the applied inflation pressure p^*. The membrane had initial radius $R = 40$ mm and thickness $H = 2$ mm.

The problem of circular membrane inflation was solved numerically following the procedure described in Appendix C.1 of Sirotti et al. (2025). A simultaneous fit of the uniaxial tension and membrane inflation data sets was carried out in MATLAB. For comparison, the constitutive models proposed by Khiêm and Itskov (2016) and Anssari-Benam (2021) were also calibrated using the same procedure. The resulting fitting parameters are given in Table B.2 and the corresponding curves are presented in Fig. 7(a) and (b).

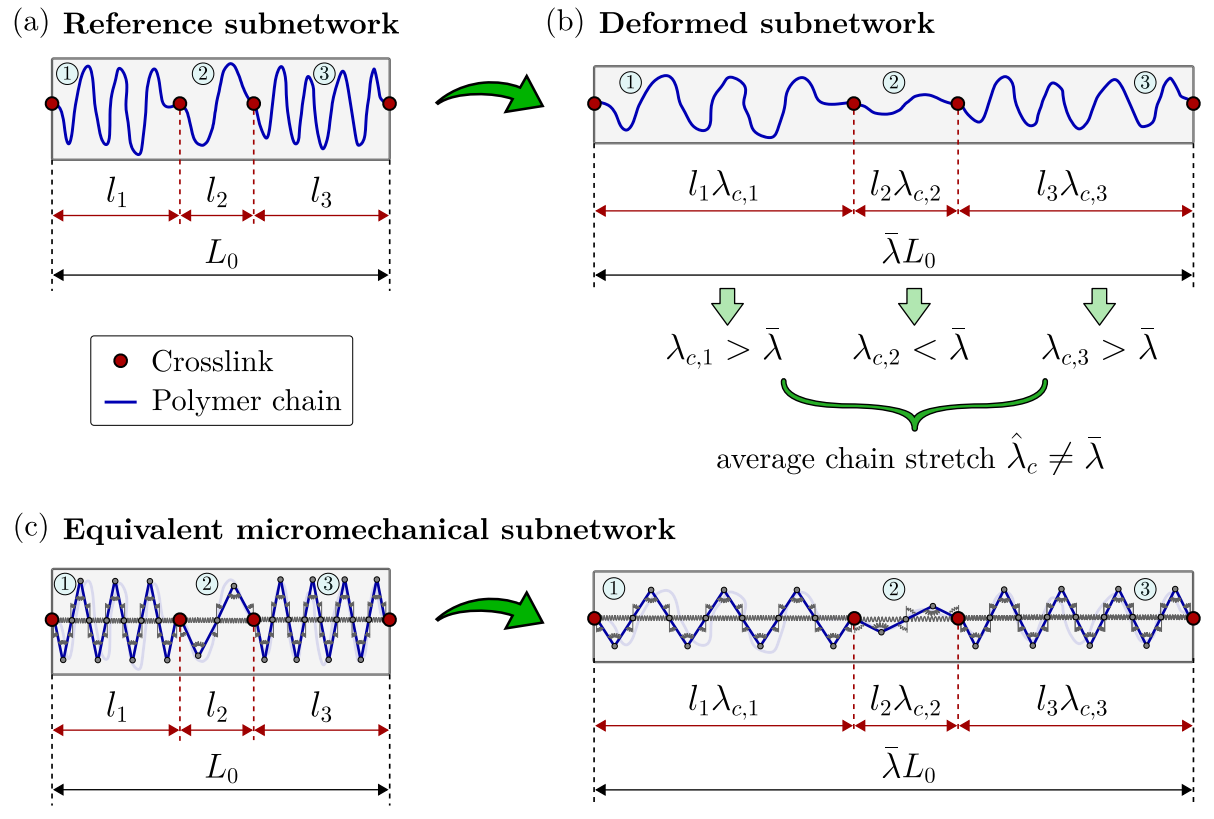

Fig. 8. Illustration of non-affine deformation in a directional polymer subnetwork composed of three chains. The reference configuration (a) deforms into the current configuration (b) under an imposed macroscopic isochoric stretch $\bar{\lambda}$. The shortest chain approaches its locking stretch and becomes stiffer, resulting in inhomogeneous chain stretches. (c) Equivalent micromechanical representation of the subnetwork in terms of the micro-structural model.

We observe that the model proposed in Anssari-Benam (2021) tends to exhibit larger discrepancies in the deformation range where finite chain extensibility becomes dominant and strain hardening plays a significant role. The present model and the formulation by Khiêm and Itskov (2016) appear to provide a more accurate representation of the response across the entire deformation regime.

Additional fitting results were examined for the case of NBR rubber, for which uniaxial data are available from Pelliciari et al. (2023). To obtain the corresponding inflation data, experimental inflation tests were conducted on circular membranes made of the same NBR, using the testing machine and experimental setup described in Section 3.2 of Sirotti et al. (2025). The membrane thickness in these tests was 0.9 mm. Simultaneous fit was then performed, yielding the parameters reported in Table B.2 and the curves shown in Fig. 7(c) and (d). In this case, the proposed model provides an improved level of accuracy compared to the other models considered.

6. Model extension to non-affine molecular network

It is generally acknowledged that the assumption of affine stretching of polymer chains becomes inappropriate in the strain regime approaching finite chain extensibility (see, for instance, Boyce and Arruda, 2000). The underlying motivation is that, in a real polymer network, when a chain is stretched close to its maximum extensibility, it deforms less than the imposed macroscopic stretch and therefore does not follow an affine deformation. At this stage, other chains in the network will stretch more than predicted by the affine kinematics in order to accommodate the applied macroscopic deformation. Moreover, polymer chain slippage through entanglements may occur, leading to additional non-affine behavior between microscopic and macroscopic deformations. As a result, the microscopic stretch may differ from the imposed macroscopic stretch, being either smaller or larger.

A visual interpretation of non-affine deformation can be obtained from Fig. 8 by considering a directional subnetwork, in line with the interpretation of Khiêm and Itskov (2016), consisting of polymer chains connected in series.

For illustrative purposes, in Fig. 8(a) we consider three polymer chains in series, where chains 1 and 3 are significantly longer than the middle chain 2. Upon application of a macroscopic stretch $\bar{\lambda}$ along the direction of the subnetwork, all three chains deform, each undergoing a stretch $\lambda_{c,i}$, with $i = 1, 2, 3$. When a sufficiently large stretch is applied, the shortest chain (chain 2) approaches its locking stretch and therefore becomes much stiffer than chains 1 and 3, which remain far from the locking regime (Fig. 8(b)). Consequently, chains 1 and 3 undergo larger deformations than chain 2 in order to accommodate the imposed macroscopic stretch

$\bar{\lambda}$. It follows that the mean chain stretch $\hat{\lambda}_c$ differs from the macroscopic stretch $\bar{\lambda}$, i.e. $\hat{\lambda}_c \neq \bar{\lambda}$. Therefore, within the framework of generalized network-averaging, this results in a non-affine deformation.

Fig. 8(c) shows the equivalent representation of the subnetwork composed of micro-structural elements connecting crosslinks and resembling polymer chains. The deformed configuration illustrates that structure 2 is much closer to its locking state than structures 1 and 3. As a result, it becomes stiffer and undergoes a smaller stretch.

To introduce non-affine deformation in the polymer network, we consider the stretch fluctuation field concept proposed by Miehe et al. (2004). Within this framework, the average micro-stretch $\hat{\lambda}_c$ is allowed to fluctuate relative to the macroscopic stretch $\bar{\lambda}$ according to $\hat{\lambda}_c = f\bar{\lambda}$, where f is a scalar fluctuation field defined on the unit sphere. A form of f was derived in Miehe et al. (2004) by minimizing the averaged free energy under the constraint that the p-root average of the non-affine chain stretch coincides with the p-root average of the macroscopic stretch. This approach requires numerical evaluation through discretization of a continuous integral over the unit sphere.

An alternative formulation for the micro–macro transition, based on stretch fluctuations inferred from experimental observations, was proposed by Heinrich et al. (1988) in the form

$$\hat{\lambda}_c = \bar{\lambda}^{\beta}, \tag{59}$$

where the exponent β depends on the degree of swelling and the extent of network imperfections. Eq. (59) has been adopted in several non-affine network theories, including those of Khiêm and Itskov (2016), Kroon (2011), Darabi and Itskov (2021), and is also employed in the present extension of our model.[4]

Regarding the micro- and macro-scale tube area contractions, non-affinity is not considered in the present formulation. Accordingly, we assume that the average microscopic tube contraction coincides with the macroscopic one, i.e. $\hat{v}_t = \bar{v}$. Consequently, non-affinity in the transition from the micro to the continuum level is entirely included in the chain stretching. We remark, however, that some authors have proposed the power-law relation $\hat{v}_t = \bar{v}^q$ (Miehe et al., 2004), where q is an additional material parameter.

The strain energy of the non-affine model is obtained by substituting the average macro-stretch $\langle\bar{\lambda}\rangle_2 = \sqrt{\bar{I}_1/3}$ into the micro–macro relation (59). The resulting expression is then evaluated by considering the contribution from chain stretching, given by (24), while the contribution from tube contraction remains as defined in (50). The explicit expression of the strain-energy function for the non-affine model thus reads

$$\tilde{W} = \tilde{W}_c(\bar{I}_1) + \tilde{W}_t(\bar{I}_2) = \frac{3\mu_c}{4\beta}\left(\frac{e^{2\alpha}\left(1 - e^{-\alpha\left(\frac{\bar{I}_1}{3}\right)^{\beta/2}}\right)^2}{\alpha(e^{\alpha}-1)} + \frac{\sqrt{n-1}\,\arcsin^2\left(\frac{1}{\sqrt{n}}\left(\frac{\bar{I}_1}{3}\right)^{\beta/2}\right)}{\arcsin\left(\frac{1}{\sqrt{n}}\right)}\right) + \mu_t\left(\sqrt{\frac{\bar{I}_2}{3}} - 1\right) + W_c^0, \tag{60}$$

where constant W_c^0 is chosen such that the reference configuration has zero energy.

6.1. Modeling capacity of the non-affine model

We consider further experimental datasets for a styrene-butadiene rubber (SBR) and a room-temperature-vulcanized (RTV) silicone, and perform a comparative fitting analysis using both the affine and non-affine versions of the proposed hyperelastic model. For SBR, the affine network assumption is expected to remain a good approximation. This material is characterized by a relatively homogeneous network, with a crosslink density and network topology comparable to those of conventional sulfur-vulcanized rubbers such as NR and NBR, for which the affine model has already demonstrated good agreement with experimental data. Under these conditions, chain-level fluctuations and network imperfections play a secondary role, and the macroscopic deformation can be approximately transmitted to the polymer chains in an affine manner.

In contrast, RTV silicones usually exhibit a markedly different network structure. Curing processes occurring at low temperature lead to networks with a higher degree of heterogeneity, including dangling chains, loops, and spatial fluctuations. Moreover, these materials typically exhibit a lower crosslink density. Such microstructural features promote non-affine chain rearrangements under deformation, thereby reducing the validity of an affine kinematic assumption. Accordingly, a non-affine description is expected to be more appropriate, whereas the affine model may fail to provide accurate fits.

To test the model in a challenging case, we consider inhomogeneous deformations by simultaneously fitting uniaxial tension and circular membrane inflation data. The SBR rubber data considered in this study are reported in Sasso et al. (2008), while the RTV silicone data are taken from Pelliciari et al. (2025). A simultaneous fitting of the uniaxial and inflation data sets was performed in MATLAB, and the resulting plots are presented in Fig. 9.

For SBR rubber, the fitted parameters of the affine model are $\mu_c = 0.9453$ MPa, $\alpha = 0.001$, $n = 7.8212$, and $\mu_t = 1.1349$ MPa, whereas the non-affine model yields $\mu_c = 0.8803$ MPa, $\alpha = 0.2105$, $n = 2 \times 10^4$, $\mu_t = 1.215$ MPa, and $\beta = 1.3$. As expected, the fitting results for

[4] Although originally introduced on phenomenological grounds, the relation (59) was micromechanically motivated by Ehret (2015), who demonstrated that a non-affine deformation of polymer chains based on a power-law dependence on the macroscopic stretch leads to Ogden's strain-energy function (Ogden, 1972) within a statistical-mechanical framework. Furthermore, for the case $\beta \leq 1$, it was shown that the exponent β represents the ratio between the microscopic and macroscopic logarithmic strains, and thus quantifies the fraction of macroscopic deformation that is elastically stored at the chain level.

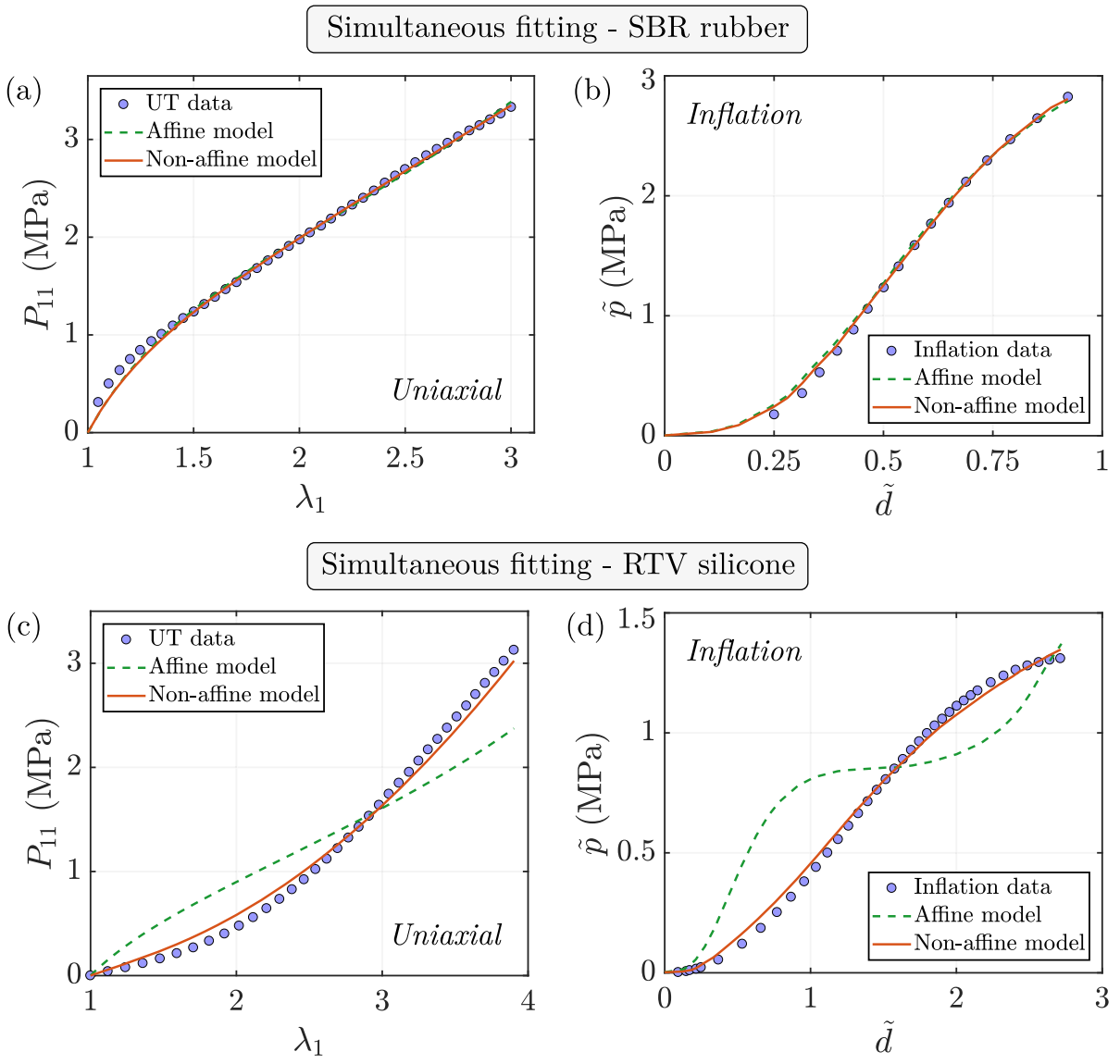

Fig. 9. Results from simultaneous fitting of affine and non-affine models to uniaxial tension and biaxial membrane inflation data for (a,b) SBR rubber, reported in Sasso et al. (2008), and (c,d) RTV silicone, from Pelliciari et al. (2025). In figures (b) and (d), deflection and pressure are normalized as $\tilde{d} = d/R$ and $\tilde{p} = p^* R/H$.

SBR confirm that the affine model, despite involving only four parameters, is able to effectively capture simultaneous stress states including inhomogeneous deformations. The additional parameter β does not lead to a significant improvement in the quality of the fit, as the results obtained with the affine and non-affine models are nearly identical.

On the other hand, for RTV silicone, the fitting parameters of the affine model are $\mu_c = 0.53$ MPa, $\alpha = 0.001$, $n = 12$, and $\mu_t = -0.195$ MPa, while for the non-affine model $\mu_c = 0.25$ MPa, $\alpha = 0.1$, $n = 10^4$, $\mu_t = -0.246$ MPa, and $\beta = 1.84$. In this case, Fig. 9(c) and (d) clearly show that the affine network assumption is not suitable. The affine model provides poor agreement with the experimental data and is unable to capture the pronounced strain hardening behavior of RTV silicone, which already develops at moderate stretches. Conversely, the introduction of the parameter β within the non-affine model allows this behavior to be accurately reproduced, together with the pressure–deflection data from membrane inflation, yielding an excellent overall fit.

We note that, in this latter application, the fitting procedure yielded a negative value of μ_t, which violates the E inequalities given in (54). Physical admissibility is therefore assessed by verifying the BE inequalities (53). A numerical evaluation over the domain $\lambda_1, \lambda_2 \in [0.5, 4]$, with λ_3 determined by incompressibility, shows that the BE inequalities are satisfied throughout this deformation range. This domain is chosen so as to cover the range of deformations within which the silicone under consideration can reasonably be assumed to exhibit an elastic response.

7. Conclusion

The proposed micromechanical model departs from the classical statistical mechanics approach while retaining essential connections to its fundamental principles. In particular, (i) the elastic structure representing the polymer chain is composed of n rigid bars, resembling Kuhn segments; (ii) the initial end-to-end length is $\sqrt{n}l$, as dictated by random-walk statistics; and (iii) the geometry of the structure naturally introduces a locking stretch $\lambda_L = \sqrt{n}$, in agreement with the non-Gaussian statistical theory.

The free energy of the chain derived from the microscale structural model admits an analytical expression and incorporates two main contributions. The first governs the response at small-to-moderate strains and arises from entanglement constraints, together with their progressive reduction under stretching. This contribution has a functional form similar to that proposed in the phenomenological model of Yeoh and Fleming (1997), although here it emerges from a micromechanical formulation. The second contribution becomes dominant at large strains and is associated with the progressive alignment of the bars, leading to a limiting chain extensibility. Its analytical form exhibits a qualitative behavior comparable to that of the inverse Langevin function, while avoiding the need for approximations.

The strain-energy function of the isotropic polymer network was derived by generalized network-averaging under the assumption of affine deformation and involves four material parameters. An extension of the formulation was also presented to account for the more general case of non-affine kinematics, introducing one additional parameter. The affine model was assessed through fitting to well-established experimental data for rubbers in biaxial tests, as well as to data involving inhomogeneous deformations from membrane inflation experiments, showing robust predictive capabilities. However, for a specific set of data for an RTV silicone, the affine deformation assumption proved inadequate. In this case, simultaneous prediction of uniaxial and inflation responses required the adoption of the non-affine model.

The main contributions and advantages of the proposed model may be summarized as follows.

- The interpretation of the polymer chain as an elastic structure enables the explicit incorporation of the mechanisms governing chain behavior in a direct and physically transparent manner. Within this structural mechanics framework, the model components, or their associated elastic potentials, may be modified to represent different mechanisms in polymer networks, providing a natural basis for extensions and generalizations with a clear microscopic interpretation.
- The parameters introduced in the model have a clear physical meaning associated with specific mechanisms. This aspect may be important for the development of constitutive descriptions in which a minimal yet sufficient set of parameters is used to capture the nonlinear elasticity of rubbers.
- The representation of entanglement effects through an exponentially decaying law motivated by the Morse potential contribute significantly to the response in the small-to-moderate deformation regime. The results obtained in this work suggest that this feature is relevant for a comprehensive constitutive model.
- For the range of rubber behaviors considered, the model provides a consistent description of multiaxial stress states and inhomogeneous deformations, which may not always be ensured in existing models.
- The analytical nature of the formulation offers convenience in theoretical developments and in the solution of elasticity problems.

Despite the advantages discussed above, the proposed model also presents some limitations. First, the effect of entanglements is represented in an effective manner through elastic elements. However, in polymer networks some entanglements may remain trapped, while others progressively release during deformation. Extensions aimed at distinguishing between these two mechanisms may be the focus of future developments. Second, the present study is limited to purely elastic behavior. Rubber-like materials however are known to exhibit inelastic effects, such as the Mullins effect, and time-dependent behavior, such as viscoelasticity. The proposed framework may thus be extended by incorporating dissipative elements within the structural representation of the polymer chain in order to account for such phenomena.

CRediT authorship contribution statement

Matteo Pelliciari: Writing – review & editing, Writing – original draft, Validation, Software, Methodology, Investigation, Funding acquisition, Formal analysis, Conceptualization; **Stefano Sirotti:** Writing – review & editing, Methodology, Investigation; **Angelo Marcello Tarantino:** Writing – review & editing, Funding acquisition.

Data availability

Data will be made available on request.

Declaration of competing interest

The authors declare that they have no known competing financial interests or personal relationships that could have appeared to influence the work reported in this paper.

Acknowledgement

This work was supported by the Italian Ministry of University and Research (MUR) through the research grants FIS 2 "PNC-Gen" (CUP E53C25000440001) and FISA-2022 "Earth-Tech" (CUP E93C24000250001). Support from the National Group of Mathematical Physics (GNFM–INdAM) is also acknowledged.

Appendix A. Collected relations for homogeneous deformations

We recall that incompressibility requires $\lambda_1\lambda_2\lambda_3 = 1$. In the following, we report the nonzero components of the nominal stress tensor for each deformation mode.

(i) Uniaxial tension. The deformation consists of stretching in direction $\mathbf{e}_1$, with the lateral stretches determined by incompressibility. The deformation gradient is

$$\mathbf{F} = \lambda_1\, \mathbf{e}_1 \otimes \mathbf{e}_1 + \lambda_1^{-1/2}\, \mathbf{e}_2 \otimes \mathbf{e}_2 + \lambda_1^{-1/2}\, \mathbf{e}_3 \otimes \mathbf{e}_3, \tag{A.1}$$

The corresponding nominal stress is

$$P_{11} = 2\left(\frac{\partial W}{\partial I_1} + \frac{1}{\lambda_1}\frac{\partial W}{\partial I_2}\right)\left(\lambda_1 - \frac{1}{\lambda_1^2}\right). \tag{A.2}$$

(ii) Equibiaxial tension. The in-plane stretches are equal and the material contracts in the normal direction:

$$\mathbf{F} = \lambda_1\, \mathbf{e}_1 \otimes \mathbf{e}_1 + \lambda_1\, \mathbf{e}_2 \otimes \mathbf{e}_2 + \lambda_1^{-2}\, \mathbf{e}_3 \otimes \mathbf{e}_3. \tag{A.3}$$

The in-plane nominal stresses reduce to

$$P_{11} = P_{22} = 2\left(\frac{\partial W}{\partial I_1} + \lambda_1^2\frac{\partial W}{\partial I_2}\right)\left(\lambda_1 - \frac{1}{\lambda_1^5}\right). \tag{A.4}$$

(iii) Biaxial tension. A general biaxial extension is described by

$$\mathbf{F} = \lambda_1\, \mathbf{e}_1 \otimes \mathbf{e}_1 + \lambda_2\, \mathbf{e}_2 \otimes \mathbf{e}_2 + (\lambda_1\lambda_2)^{-1}\, \mathbf{e}_3 \otimes \mathbf{e}_3. \tag{A.5}$$

The nominal stresses are

$$\begin{aligned} P_{11} &= 2\left(\frac{\partial W}{\partial I_1} + \lambda_2^2\frac{\partial W}{\partial I_2}\right)\left(\lambda_1 - \frac{1}{\lambda_1^3\lambda_2^2}\right), \\ P_{22} &= 2\left(\frac{\partial W}{\partial I_1} + \lambda_1^2\frac{\partial W}{\partial I_2}\right)\left(\lambda_2 - \frac{1}{\lambda_1^2\lambda_2^3}\right). \end{aligned} \tag{A.6}$$

(iv) Pure shear. Pure shear is described by the deformation gradient

$$\mathbf{F} = \lambda_1\, \mathbf{e}_1 \otimes \mathbf{e}_1 + \mathbf{e}_2 \otimes \mathbf{e}_2 + \lambda_1^{-1}\mathbf{e}_3 \otimes \mathbf{e}_3. \tag{A.7}$$

The corresponding nominal stresses are

$$\begin{aligned} P_{11} &= 2\left(\frac{\partial W}{\partial I_1} + \frac{\partial W}{\partial I_2}\right)\left(\lambda_1 - \frac{1}{\lambda_1^3}\right), \\ P_{22} &= 2\left(\frac{\partial W}{\partial I_1} + \lambda_1^2\frac{\partial W}{\partial I_2}\right)\left(1 - \frac{1}{\lambda_1^2}\right). \end{aligned} \tag{A.8}$$

Appendix B. Fitting parameters

The material parameters obtained from fitting the uniaxial tension data shown in Fig. 6 are listed in Table B.1. The parameters obtained from the simultaneous fitting of the uniaxial and inflation data shown in Fig. 7 are reported in Table B.2.

Table B.1
Material parameters obtained by fitting the present model (51), the model in (56) by Khiêm and Itskov (2016), and the model in (57) by Anssari-Benam (2021) to the uniaxial tension data reported in Pelliciari et al. (2023). Where applicable, values are expressed in MPa.

Material	Model	Parameters			
EPDM	Khiêm–Itskov	$\mu_c\kappa = 0.3361$	$q = 1.083$	$n = 54.2$	$\mu_t = 3.876$
	Anssari-Benam	$\mu = 0.5765$	$\bar{n} = 1.095$	$N = 17.84$	$C_2 = 1.633$
	Present model	$\mu_c = 0.9691$	$\alpha = 35.49$	$n = 35.1$	$\mu_t = 3.293$
NBR	Khiêm–Itskov	$\mu_c\kappa = 0.05139$	$q = 3.627$	$n = 10^4$	$\mu_t = 14.68$
	Anssari-Benam	$\mu = 2.752$	$\bar{n} = 0.9741$	$N = 0.9885$	$C_2 = 2 \times 10^{-14}$
	Present model	$\mu_c = 5.844$	$\alpha = 31.64$	$n = 10^4$	$\mu_t = 0.1627$
NR	Khiêm–Itskov	$\mu_c\kappa = 0.3438$	$q = 1.193$	$n = 33.27$	$\mu_t = 1.119$
	Anssari-Benam	$\mu = 0.5738$	$\bar{n} = 95.65$	$N = 20.16$	$C_2 = 0.2245$
	Present model	$\mu_c = 1.249$	$\alpha = 81.29$	$n = 15.76$	$\mu_t = 0.1785$
Silicone	Khiêm–Itskov	$\mu_c\kappa = 0.2988$	$q = 1.571$	$n = 10^4$	$\mu_t = 1.954$
	Anssari-Benam	$\mu = 34.9$	$\bar{n} = 22.82$	$N = 0.0855$	$C_2 = 5.102$
	Present model	$\mu_c = 1.839$	$\alpha = 64.61$	$n = 8.742$	$\mu_t = 2 \times 10^{-14}$

Table B.2
Material parameters obtained by simultaneous fitting of the present model (51), the model in (56) by Khiêm and Itskov (2016), and the model in (57) by Anssari-Benam (2021) to uniaxial tension and biaxial membrane inflation data for NR and NBR rubbers. Where applicable, values are expressed in MPa.

Material	Model	Parameters			
NR	Khiêm–Itskov	$\mu_c\kappa = 0.54$	$q = 1.06$	$n = 30$	$\mu_t = 0.0001$
	Anssari-Benam	$\mu = 0.61$	$\bar{n} = 50$	$N = 18$	$C_2 = 10^{-10}$
	Present model	$\mu_c = 1.34$	$\alpha = 97$	$n = 20.5$	$\mu_t = 0.0003$
NBR	Khiêm–Itskov	$\mu_c\kappa = 2.85$	$q = 0.95$	$n = 15$	$\mu_t = 0.05$
	Anssari-Benam	$\mu = 2.666$	$\bar{n} = 0.978$	$N = 0.9907$	$C_2 = 0.5$
	Present model	$\mu_c = 5.8$	$\alpha = 29.5$	$n = 20$	$\mu_t = 0.1911$

References

Anssari-Benam, A., 2021. On a new class of non-Gaussian molecular-based constitutive models with limiting chain extensibility for incompressible rubber-like materials. Math. Mech. Solids 26 (11), 1660–1674.

Anssari-Benam, A., 2024. Hyperinelasticity: an energy-based constitutive modelling approach to isothermal large inelastic deformation of polymers. Part I. J. Mech. Phys. Solids 192, 105790.

Anssari-Benam, A., Bucchi, A., 2021. A generalised neo-Hookean strain energy function for application to the finite deformation of elastomers. Int. J. Non-Linear Mech. 128, 103626.

Anssari-Benam, A., Bucchi, A., Saccomandi, G., 2021. On the central role of the invariant I_2 in nonlinear elasticity. Int. J. Eng. Sci. 163, 103486.

Anssari-Benam, A., Horgan, C.O., 2022. A three-parameter structurally motivated robust constitutive model for isotropic incompressible unfilled and filled rubber-like materials. Eur. J. Mech.-A/Solids 95, 104605.

Arruda, E.M., Boyce, M.C., 1993. A three-dimensional constitutive model for the large stretch behavior of rubber elastic materials. J. Mech. Phys. Solids 41 (2), 389–412.

Baker, M., Ericksen, J.L., 1954. Inequalities restricting the form of the stress-deformation relations for isotropic elastic solids and Reiner-Rivlin fluids. J. Wash. Acad. Sci. 44 (2), 33–35.

Beatty, M.F., 2003. An average-stretch full-network model for rubber elasticity. J. Elast. 70 (1), 65–86.

Bischoff, J.E., Arruda, E.M., Grosh, K., 2001. A new constitutive model for the compressibility of elastomers at finite deformations. Rubber Chem. Technol. 74 (4), 541–559.

Boyce, M.C., Arruda, E.M., 2000. Constitutive models of rubber elasticity: a review. Rubber Chem. Technol. 73 (3), 504–523.

Cohen, A., 1991. A Padé approximant to the inverse Langevin function. Rheol. Acta 30 (3), 270–273.

Currie, P.K., 2004. The attainable region of strain-invariant space for elastic materials. Int. J. Non-Linear Mech. 39 (5), 833–842.

Dal, H., Açıkgöz, K., Badienia, Y., 2021. On the performance of isotropic hyperelastic constitutive models for rubber-like materials: a state of the art review. Appl. Mech. Rev. 73 (2), 020802.

Dal, H., Gültekin, O., Açıkgöz, K., 2020. An extended eight-chain model for hyperelastic and finite viscoelastic response of rubberlike materials: theory, experiments and numerical aspects. J. Mech. Phys. Solids 145, 104159.

Darabi, E., Itskov, M., 2021. A generalized tube model of rubber elasticity. Soft Matter 17 (6), 1675–1684.

Destrade, M., Saccomandi, G., Sgura, I., 2017. Methodical fitting for mathematical models of rubber-like materials. Proc. R. Soc. A Math. Phys. Eng. Sci. 473 (2198), 20160811.

Doi, M., Edwards, S.F., 1986. The Theory of Polymer Dynamics. Clarendon Press, Oxford.

Ehret, A.E., 2015. On a molecular statistical basis for Ogden's model of rubber elasticity. J. Mech. Phys. Solids 78, 249–268.

Falope, F.O., Lanzoni, L., Tarantino, A.M., 2024. Energetic exhaustiveness for the direct characterization of energy forms of hyperelastic isotropic materials. J. Mech. Phys. Solids 193, 105885.

Flory, P.J., Rehner, J., 1943. Statistical mechanics of cross-linked polymer networks II. Swelling. J. Chem. Phys. 11 (11), 521–526.

Gartner III, T.E., Jayaraman, A., 2019. Modeling and simulations of polymers: a roadmap. Macromolecules 52 (3), 755–786.

Guth, E., Mark, H., 1934. Zur innermolekularen, Statistik, insbesondere bei Kettenmolekiilen I. Monatshefte für Chemie und verwandte Teile anderer Wissenschaften 65 (1), 93–121.

Heinrich, G., Straube, E., Helmis, G., 1988. Rubber elasticity of polymer networks: theories. In: Polymer Physics. Springer Berlin Heidelberg, Berlin, Heidelberg, pp. 33–87.

Horgan, C.O., Saccomandi, G., 2002. A molecular-statistical basis for the Gent constitutive model of rubber elasticity. J. Elast. 68 (1), 167–176.

Horgan, C.O., Saccomandi, G., 2004. Constitutive models for compressible nonlinearly elastic materials with limiting chain extensibility. J. Elast. 77, 123–138.
James, H.M., Guth, E., 1943. Theory of the elastic properties of rubber. J. Chem. Phys. 11 (10), 455–481.
Kawabata, S., Matsuda, M., Tei, K., Kawai, H., 1981. Experimental survey of the strain energy density function of isoprene rubber vulcanizate. Macromolecules 14 (1), 154–162.
Kearsley, E.A., 1989. Note: strain invariants expressed as average stretches. J. Rheol. 33 (5), 757–760.
Khiêm, V.N., Itskov, M., 2016. Analytical network-averaging of the tube model: rubber elasticity. J. Mech. Phys. Solids 95, 254–269.
Kroon, M., 2011. An 8-chain model for rubber-like materials accounting for non-affine chain deformations and topological constraints. J. Elast. 102 (2), 99–116.
Kuhn, W., 1934. Über die gestalt fadenförmiger moleküle in lösungen. Kolloid-Z. 68 (1), 2–15.
Kuhn, W., Grün, F., 1942. Beziehungen zwischen elastischen Konstanten und Dehnungsdoppelbrechung hochelastischer Stoffe. Kolloid-Z. 101 (3), 248–271.
Lavoie, S.R., Long, R., Tang, T., 2019. Modeling the mechanics of polymer chains with deformable and active bonds. J. Phys. Chem. B 124 (1), 253–265.
Marckmann, G., Verron, E., 2006. Comparison of hyperelastic models for rubber-like materials. Rubber Chem. Technol. 79 (5), 835–858.
Marzano, S., 1983. An interpretation of Baker-Ericksen inequalities in uniaxial deformation and stress. Meccanica 18 (4), 233–235.
Meunier, L., Chagnon, G., Favier, D., Orgéas, L., Vacher, P., 2008. Mechanical experimental characterisation and numerical modelling of an unfilled silicone rubber. Polym. Test. 27 (6), 765–777.
Miehe, C., Göktepe, S., Lulei, F., 2004. A micro-macro approach to rubber-like materials—Part I: the non-affine micro-sphere model of rubber elasticity. J. Mech. Phys. Solids 52 (11), 2617–2660.
Mihai, L.A., Goriely, A., 2017. How to characterize a nonlinear elastic material? A review on nonlinear constitutive parameters in isotropic finite elasticity. Proc. R. Soc. A Math. Phys. Eng. Sci. 473 (2207), 20170607.
Ogden, R.W., 1972. Large deformation isotropic elasticity – on the correlation of theory and experiment for incompressible rubberlike solids. Proc. R. Soc. London A Math. Phys. Sci. 326 (1567), 565–584.
Ogden, R.W., Saccomandi, G., Sgura, I., 2004. Fitting hyperelastic models to experimental data. Comput. Mech. 34, 484–502.
Pelliciari, M., Sirotti, S., Aloisio, A., Tarantino, A.M., 2025. Hyperelastic model for nonlinear elastic deformations of graphene-based polymer nanocomposites. Int. J. Solids Struct. 308, 113144.
Pelliciari, M., Sirotti, S., Tarantino, A.M., 2023. A strain energy function for large deformations of compressible elastomers. J. Mech. Phys. Solids 176, 105308.
Puthur, R., Sebastian, K.L., 2002. Theory of polymer breaking under tension. Phys. Rev. B 66 (2), 24304.
Rivlin, R.S., Ericksen, J.L., 1997. Stress–deformation relations for isotropic materials. In: Barenblatt, G.I., Joseph, D.D. (Eds.), Collected Papers of R. S. Rivlin: Volume I and II. Springer, pp. 911–1013.
Sansour, C., 2008. On the physical assumptions underlying the volumetric-isochoric split and the case of anisotropy. Eur. J. Mech.-A/Solids 27 (1), 28–39.
Sasso, M., Palmieri, G., Chiappini, G., Amodio, D., 2008. Characterization of hyperelastic rubber-like materials by biaxial and uniaxial stretching tests based on optical methods. Polym. Test. 27 (8), 995–1004.
Sirotti, S., Pelliciari, M., Aloisio, A., Tarantino, A.M., 2025. A strain energy function for the inflation of hyperelastic membranes. Mech. Mater. 209, 105442.
Steinmann, P., Hossain, M., Possart, G., 2012. Hyperelastic models for rubber-like materials: consistent tangent operators and suitability for Treloar's data. Arch. Appl. Mech. 82, 1183–1217.
Thiel, C., Voss, J., Martin, R.J., Neff, P., 2019. Do we need Truesdell's empirical inequalities? On the coaxiality of stress and stretch. Int. J. Non-Linear Mech. 112, 106–116.
Treloar, L.R.G., 1944. Stress-strain data for vulcanised rubber under various types of deformation. Trans. Faraday Soc. 40, 59–70.
Treloar, L. R.G., 1946. The statistical length of long-chain molecules. Trans. Faraday Soc. 42, 77–82.
Treloar, L.R.G., 1975. The Physics of Rubber Elasticity. Oxford University Press.
Treloar, L.R.G., Riding, G., 1979. A non-Gaussian theory for rubber in biaxial strain. I. Mechanical properties. Proc. R. Soc. London A Math. Phys. Sci. 369 (1737), 261–280.
Truesdell, C., 1952. The mechanical foundations of elasticity and fluid dynamics. J. Ration. Mech. Anal. 1, 125–300.
Truesdell, C., Noll, W., 1965. The non-linear field theories of mechanics. In: Flügge, S. (Ed.), Handbuch der Physik. Springer, Heidelberg. Vol. III/3.
Urayama, K., 2006. An experimentalist's view of the physics of rubber elasticity. J. Polym. Sci. Part B Polym. Phys. 44 (24), 3440–3444.
Wang, M.C., Guth, E., 1952. Statistical theory of networks of non-Gaussian flexible chains. J. Chem. Phys. 20 (7), 1144–1157.
Wu, P.D., Van Der Giessen, E., 1993. On improved network models for rubber elasticity and their applications to orientation hardening in glassy polymers. J. Mech. Phys. Solids 41 (3), 427–456.
Yeoh, O.H., 1993. Some forms of the strain energy function for rubber. Rubber Chem. Technol. 66 (5), 754–771.
Yeoh, O.H., Fleming, P.D., 1997. A new attempt to reconcile the statistical and phenomenological theories of rubber elasticity. J. Polym. Sci. B Polym. Phys. 35 (12), 1919–1931.